10-1-2022

Upper-Plate Structure and Tsunamigenic Faults Near the Kodiak Islands, Alaska, USA

Marlon D. Ramos
Boise State University

Lee M. Liberty
Boise State University

Peter J. Haeussler
U.S. Geological Survey

Robert Humphreys
U.S. Geological Survey

Research Paper

GEOSPHERE

GEOSPHERE, v. 18, no. 5

https://doi.org/10.1130/GES02486.1

8 figures; 1 table

CORRESPONDENCE: ramosmd@umich.edu

CITATION: Ramos, M.D., Liberty, L.M., Haeussler, P.J., and Humphreys, R., 2022, Upper-plate structure and tsunamigenic faults near the Kodiak Islands, Alaska, USA: Geosphere, v. 18, no. 5, p. 1474–1491, https://doi.org/10.1130/GES02486.1.

Science Editors: Shanaka de Silva
Christopher J. Spencer
Associate Editor: Craig H. Jones

Received 17 September 2021
Revision received 11 February 2022
Accepted 5 May 2022

Published online 12 July 2022

Upper-plate structure and tsunamigenic faults near the Kodiak Islands, Alaska, USA

Marlon D. Ramos[1,2], Lee M. Liberty[2], Peter J. Haeussler[3], and Robert Humphreys[3]

[1]Department of Earth and Environmental Sciences, University of Michigan, 1100 North University Avenue, Ann Arbor, Michigan 48109-1005, USA
[2]Department of Geosciences, Boise State University, 1910 University Drive, MS 1535, Boise, Idaho 83725-1535, USA
[3]U.S. Geological Survey, 4210 University Drive, Anchorage, Alaska 99508, USA

ABSTRACT

The Kodiak Islands lie near the southern terminus of the 1964 Great Alaska earthquake rupture area and within the Kodiak subduction zone segment. Both local and trans-Pacific tsunamis were generated during this devastating megathrust event, but the local tsunami source region and the causative faults are poorly understood. We provide an updated view of the tsunami and earthquake hazard for the Kodiak Islands region through tsunami modeling and geophysical data analysis. Using seismic and bathymetric data, we characterize a regionally extensive seafloor lineament related to the Kodiak shelf fault zone, with focused uplift along a 50-km-long portion of the newly named Ugak fault as the most likely source of the local Kodiak Islands tsunami in 1964. We present evidence of Holocene motion along the Albatross Banks fault zone, but we suggest that this fault did not produce a tsunami in 1964. We relate major structural boundaries to active forearc splay faults, where tectonic uplift is collocated with gravity lineations. Differences in interseismic locking, seismicity rates, and potential field signatures argue for different stress conditions at depth near presumed segment boundaries. We find that the Kodiak segment boundaries have a clear geophysical expression and are linked to upper-plate structure and splay faulting. The tsunamigenic fault hazard is higher for the Kodiak shelf fault zone when compared to the nearby Albatross Banks fault zone, suggesting short wave travel paths and little tsunami warning time for nearby communities.

INTRODUCTION

Nearly the entire ~4000-km-long Alaska-Aleutian subduction zone has ruptured in tsunamigenic M>8 earthquakes during the past century (Plafker, 1969; Carver and Plafker, 2008; Ryan et al., 2011). Spatial and temporal distributions of these large earthquakes have given rise to the notion that the subduction zone is segmented (Nishenko and Jacob, 1990), with the presumption that different portions of the fault have unique earthquake cycles. The last rupture near the Kodiak Islands resulted from the M9.2 1964 Great Alaska Earthquake (GAE; Fig. 1). This earthquake initiated from the slip patch, or asperity, affiliated with the Prince William Sound (PWS) segment, where uplift of up to 12 m was measured along the Patton Bay splay fault system (Plafker, 1969; Liberty et al., 2013). The slip extended through the Kenai segment (Suito and Freymueller, 2009) and terminated ~700 km to the southwest, beyond the Kodiak Islands (Johnson et al., 1996; Ichinose et al., 2007).

On the Kodiak Islands, local tsunami run-up was observed in 1964 (Kachadoorian and Plafker, 1967; Fig. 2), but seafloor displacements were not identified. The paleoseismic record shows evidence for many M8+ Holocene megathrust earthquakes associated with the Kodiak and adjacent segments (Nishenko and Jacob, 1990; Hutchinson and Crowell, 2007; Carver and Plafker, 2008; Briggs et al., 2014; Shennan et al., 2014, 2018), but the location, geometry, and slip history of faults that splay from the megathrust are unknown. Given the robust paleoseismic evidence of large megathrust earthquakes, understanding this region's fault kinematics are important to seismic and tsunami hazard analysis and risk mitigation.

As most of the Gulf of Alaska forearc is submerged (Fig. 1), paleoseismic studies have mostly relied on land elevation changes and the coastal sediment record to extract regional subsidence and uplift signals from earthquakes. However, these records do not uniquely constrain earthquake sources, cumulative slip estimates, or along-strike rupture limits from past earthquakes. Modern seismic, geodetic, and paleoseismic data suggest that M7+ earthquakes occur near the Kodiak Islands region every few decades, tsunami-capable M8 earthquakes have a median return-period of a hundred or more years, and multi-segment M9 great earthquakes have even longer return periods (Shennan et al., 2014). This temporal mismatch in coseismic behavior between the Kodiak segment and neighboring subduction zone segments suggests differences in strain accumulation and release along the plate interface which may be preserved in upper-plate structures. The potential drivers of segmented megathrust ruptures and upper-plate deformation may stem from the subduction of rough seafloor topography (e.g., seamounts, fracture zones) or variable sediment volume and associated fluid content. Geophysical data have the potential to map active faults and to characterize along-strike variations in upper- and lower-plate structures that may uncover millennial-scale seismic behaviors.

In this paper, we identify and characterize faults in the region of the Kodiak segment using legacy and new bathymetric, seismic, and potential field

Marlon D. Ramos https://orcid.org/0000-0003-4449-8624

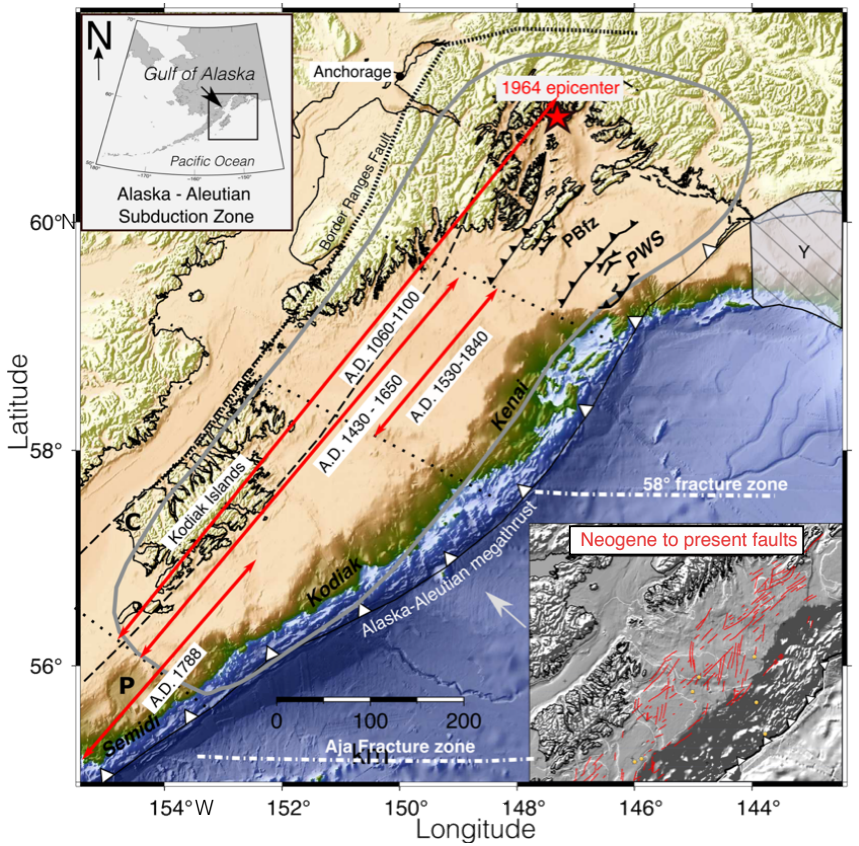

Figure 1. Great Alaska earthquake (GAE) rupture area (gray line) with shaded relief topography of the Gulf of Alaska region. Arrows denote rupture extent and age of previous megathrust earthquakes (e.g., Carver and Plafker, 2008; Briggs et al. 2014; Shennan et al., 2014). Patton Bay fault zone (PBfz) near Prince William Sound (Liberty et al., 2019) represents the region of maximum uplift during the GAE. Dotted black lines denote inferred subduction zone segment boundaries (Nishenko and Jacob, 1990; Suito and Freymueller, 2009). Inset map shows Neogene and active seafloor scarps interpreted as mostly reactivated reverse or thrust faults (red lines). Major fracture zone structures subducting below the Kodiak forearc include the Aja and 58°N fracture zones. Top inset represents the greater Alaska-Aleutian subduction zone. P—Prince William Sound terrane, C—Chugach terrane, Y—Yakutat terrane. Color map from Crameri and Shephard (2018).

data sets. We relate motion on these faults to both the GAE and other post–Last Glacial Maxima (LGM) Holocene earthquakes. We use the distribution of mapped faults to characterize upper-plate structure and to constrain the asperity boundaries and potential earthquake rupture limits. We use bathymetry data to back-project first-arrival tsunami travel times that were recorded during the 1964 earthquake and to identify tectonic scarps. We identify the faults that lie beneath these scarps with seismic-reflection data and estimate splay fault geometries and uplift rates from these data. Finally, we use satellite free-air gravity and EMAG2 magnetic anomaly data sets (Maus, 2009; Sandwell et al., 2014) to infer upper-plate deformation and assess signatures of segmentation around the Kodiak Islands.

TECTONIC SETTING

Tsunamigenic splay faults have been imaged within the Gulf of Alaska forearc with seismic and bathymetric data (von Huene et al., 2012; Liberty et al., 2013; Haeussler et al., 2015; Li et al., 2018; Liberty et al., 2019). Similar fault geometries and seafloor uplift patterns presumably span the length of this subduction zone, but differences in plate geometry and subducting structure may give rise to differences in forearc structures and earthquake potential. From teleseismic receiver function and crustal-scale, active-source seismic data across the Gulf of Alaska, we know that faults splay from the subduction interface where this megathrust dips to the north between 3°–9° (Moore et al., 1991; Eberhart-Phillips et al., 2006; Liberty et al., 2013; Kim et al., 2014; Haeussler et al., 2015; Bécel et al., 2017, Hayes et al., 2018).

The Kodiak Shelf fault zone (KSfz) and Albatross Banks fault zone (ABfz) have been inferred to control upper-plate fault motions near the Kodiak Islands (Fig. 2; Fisher and von Huene, 1980; von Huene et al., 1980; Moore et al., 1991; Carver et al., 2008). Although no direct evidence has tied the KSfz and ABfz to the megathrust, we can presume that they splay from this boundary because of their similarity to splay fault structures already imaged on nearby subduction zone segments (e.g., Moore et al., 1991; Liberty et al., 2013; Haeussler et al., 2015; Bécel et al., 2017).

Carver et al. (2008) mapped the on-land portion of the KSfz, and they named the largest fault the Narrow Cape fault. They determined a recurrence interval for surface displacing events on the fault of 1–2 k.y., or more than five times longer than the average maximum recurrence interval for M>8 earthquakes on the Kodiak segment (e.g., Shennan et al., 2018). This suggests other faults may activate during large megathrust earthquakes. The trenchward ABfz has been seismically imaged close to the continental shelf break and contains forearc basin-bounding reverse faults (Fig. 2; Fisher, 1980; Fisher and von Huene, 1980). However, slip and

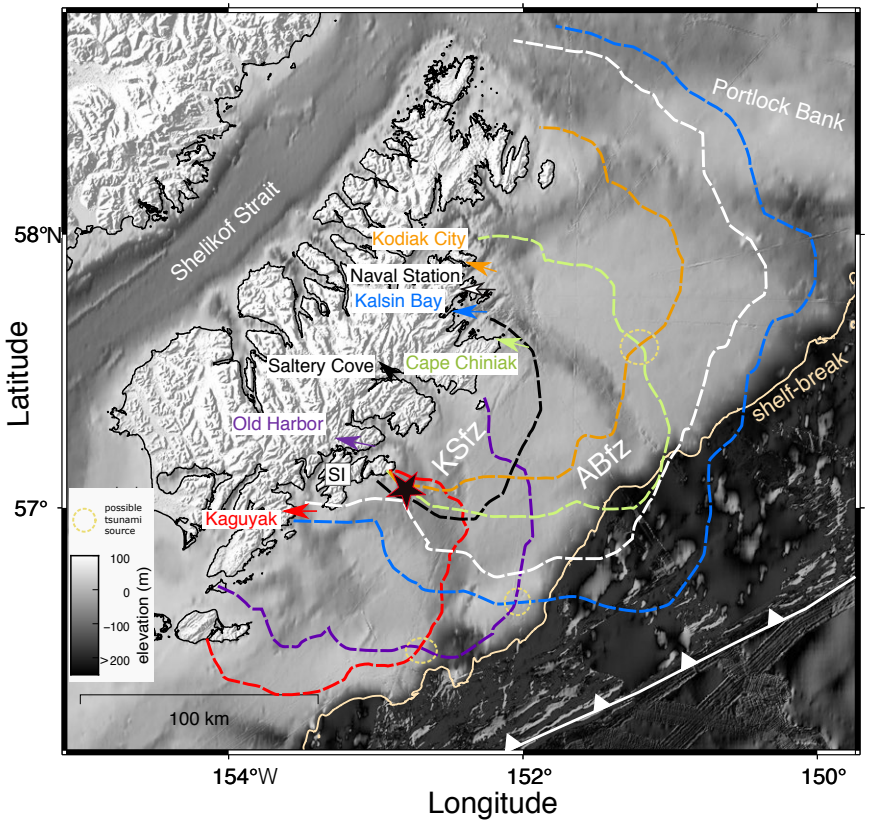

Figure 2. Results from tsunami travel-time modeling along seven run-up locations across the Kodiak Islands. Back-propagated wave fronts are colored according to run-up location and represent the maximum tsunami origin distance based on the first-arriving wave crest. The star represents the estimated convergence region belonging to five tsunami wave fronts and our preferred tsunami source that is ~15 km south of Sitkalidak Island. We term this tsunami-generating fault the Ugak fault. SI—Sitkinak Island; KSfz—Kodiak Shelf fault zone; ABfz—Albatross Banks fault zone.

fault distributions were poorly constrained due to a lack of modern seismic imagery; and there is no direct evidence that this fault system is active. In contrast, splay faults associated with the PWS and Semidi segments have been better characterized with more modern seismic and bathymetry surveys (e.g., Brocher et al., 1994; Liberty et al., 2013, 2019; Finn et al., 2015; Haeussler et al., 2015; Li et al., 2018; Shillington et al., 2015; Bécel et al., 2017). Here, we revisit legacy seismic data sets and complement these older data with newly acquired seismic data to better constrain the tectonic history of the Kodiak segment.

KODIAK SHELF BATHYMETRY

For our tsunami source and fault mapping analysis, we utilize a regional bathymetry data set to identify Kodiak shelf seafloor scarps (NOAA National Centers for Environmental Information, 2004). The Southern Alaska Coastal Relief model for most of the continental shelf was compiled at a resolution of 24 arc-seconds, or a 720 m grid interval. We complement the regional bathymetry data set with higher-resolution, 8-arc second bathymetry data, and from a new compilation that covers the western Kodiak Islands region (Zimmermann et al., 2019). We recognize that much of the continental shelf region has not been surveyed within the past 50 years, thus limiting our analyses. Regardless, our compilation shows that seafloor scarps related to the KSfz extend for at least 200 km, from offshore Sitkinak Island northeast to at least the Chiniak trough (Fig. 3). These scarps are upwards of 50 m tall, greatest in height near Sitkalidak Island.

Most of Alaska's continental shelf has water depths of 100 m or less and has been shaped by LGM ice loads, postglacial deposition, and Holocene tectonism. Sea levels were ~120 m below modern levels during the LGM (e.g., Peltier and Fairbanks, 2006), and ice covered much of the continental shelf (Kaufman and Manley, 2004; Kaufman et al., 2011). Radiocarbon dating at Narrow Cape indicates it was deglaciated ca. 13.5–13 ka (Fig. 2 and 3B; Carver et al., 2008), likely resetting seafloor surface prior to that time.

The shallow shelf areas typically contain little unconsolidated sediment that reflects modern deposition. In contrast, cross-shelf glacial troughs are often more than 50 m deeper than the nominal shelf depth and are traps for modern deposition (e.g., Carlson and Molnia, 1975; Liberty et al., 2013, 2019). These unconsolidated sediments typically lie above a prominent shallow unconformity that likely represents the hiatus in deposition during glaciation (e.g., Fig. 4E). Because many seafloor lineaments cross pre-Pleistocene depositional fabric, we assume that these lineaments represent scarps from Holocene fault uplift (e.g., Liberty et al., 2013, 2019).

FIRST-ARRIVAL 1964 TSUNAMI SOURCE

The 1964 GAE generated tsunamis that inundated shorelines around the Pacific Ocean. Plafker (1969) inferred a tsunami source from

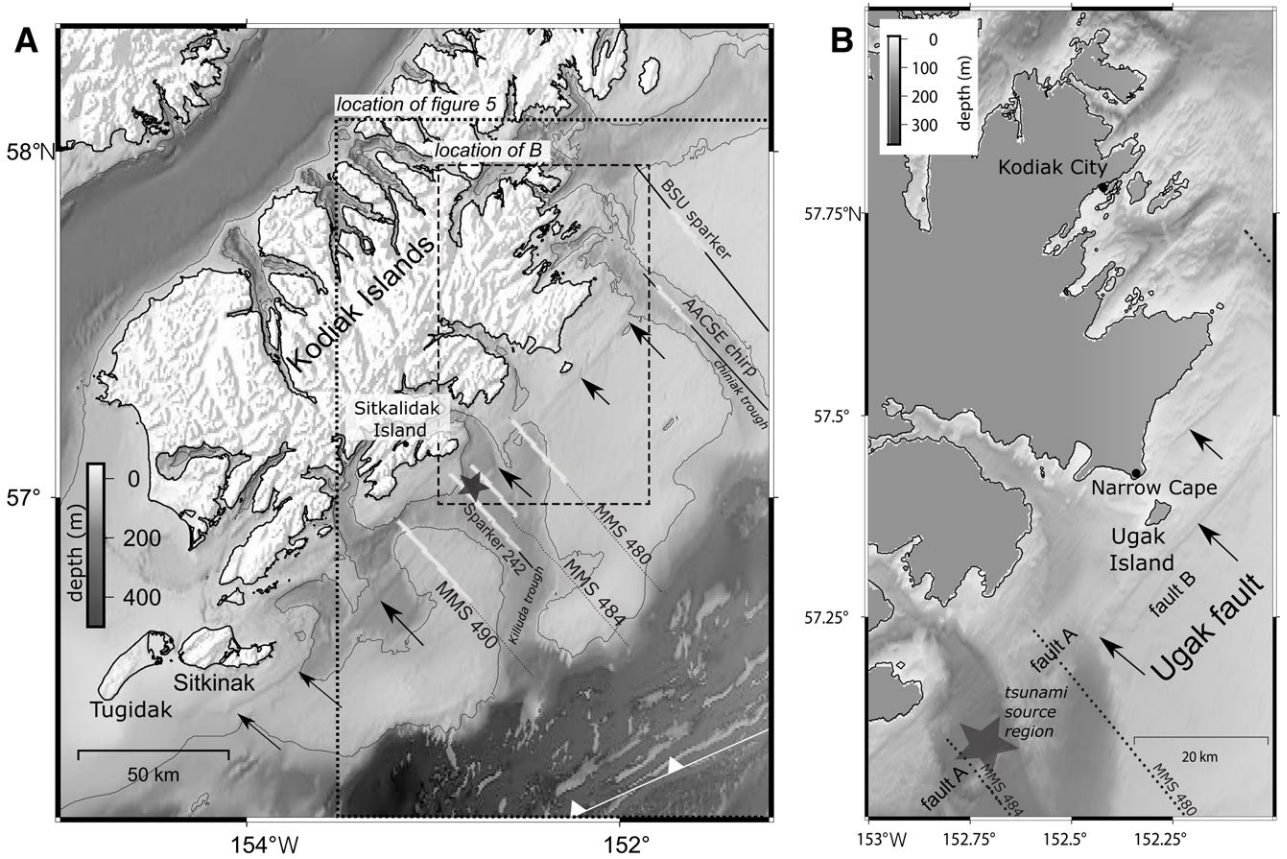

Figure 3. Kodiak Islands Shelf fault zone and related faults. (A) Twenty-four-arc second global bathymetry data with 100-m-depth bathymetric contour. The map shows prominent NE-SW–trending lineations belonging to the Kodiak Shelf fault zone (KSfz). Arrows identify prominent KSfz seafloor scarps. Labeled are seismic profiles (dark lines) and portions of the profiles presented in Figure 4 (white lines). The spatial location of Figure 3B is denoted by the dashed line, whereas Figure 5 is denoted by a dotted line. (B) Eight arc-sec bathymetry data in the dashed area of (A) showing ~20-m-high Ugak and related faults highlighted with the seismic profiles. Gray region indicates land. Star represents our preferred 1964 tsunami source location.

the continuation of the Patton Bay fault to have caused the first waves that arrived on the Kodiak Islands (Fig. 2 and Table 1). However, the offshore extension of the Patton Bay fault was not mapped at that time. Subsequently, Liberty et al. (2019) showed that Holocene activity along the Patton Bay fault system diminishes to the southwest of PWS as large scarps do not extend across the Kenai segment (Liberty, 2015; Fig. 1). Suleimani and Freymueller (2020) evaluated the role of splay faults and horizontal displacements from several regional coseismic slip models from the GAE and found they both locally had significant contributions.

To identify coseismic uplift near the Kodiak Islands, we use modern bathymetry (Fig. 3), seismic-reflection data (Fig. 4), and a compilation of GAE tsunami first-arrival times (Table 1). We use tsunami first motions (estimated to the nearest minute) observed at seven sites on the Kodiak Islands relative to the main shock origin time (Plafker, 1969). We treat each run-up location as a wave source and back-propagate this source using finite differences (Fig. 2). To derive a velocity field, we grid multi-beam and single-beam bathymetry data at one-kilometer spacing and then convert depth to tsunami wave speed in each cell. We use La Grange's velocity-depth relationship, $v = \sqrt{gd}$, where d is the depth in meters, and g is gravitational acceleration (Lamb, 1932). Each source is then back-propagated using this velocity field according to its respective tabulated

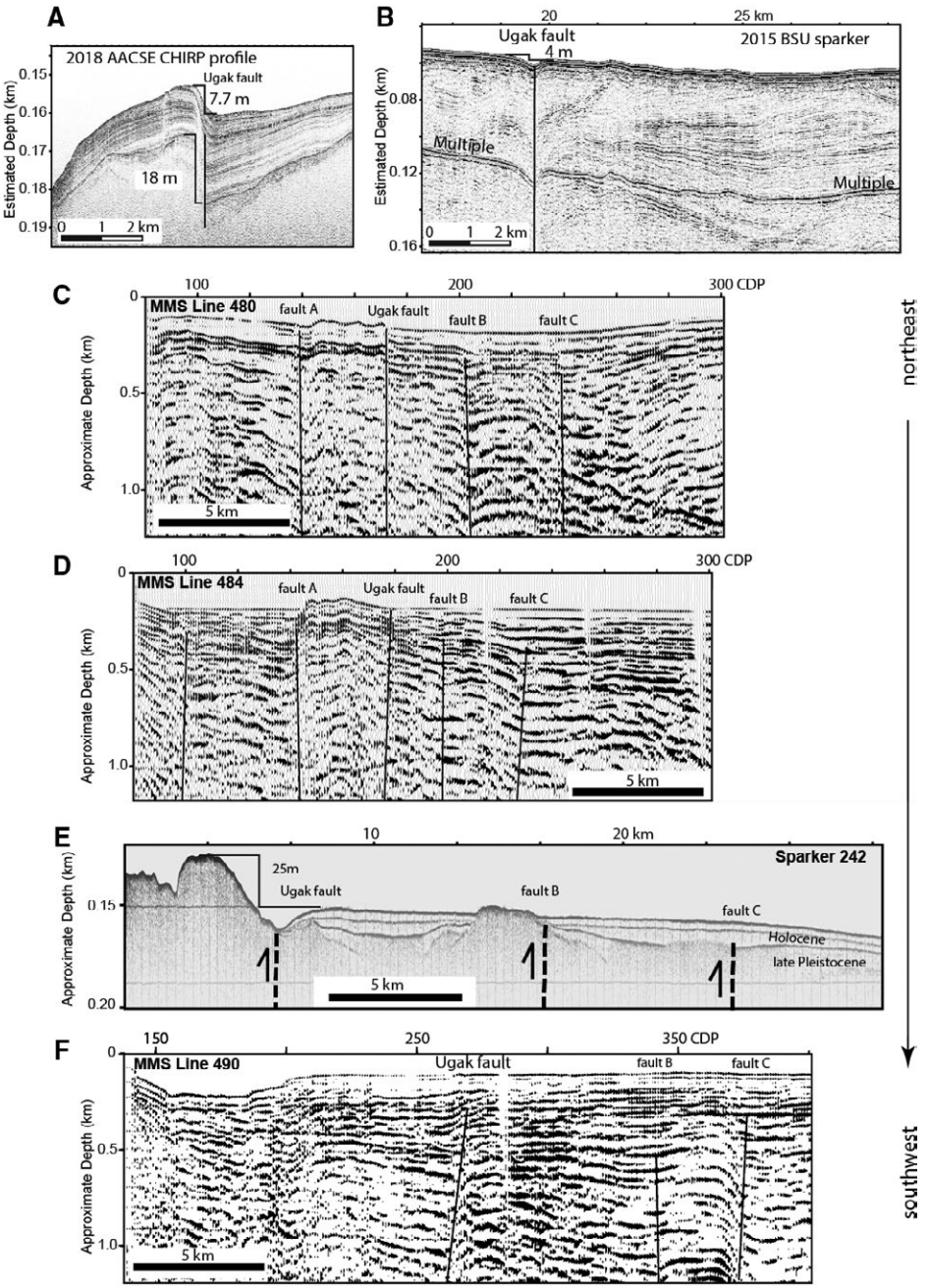

Figure 4. Chirp (A, B), Minerals Management Service (MMS) (C, D, F), and sparker (E) seismic-reflection profiles that cross the Ugak fault. Locations are noted on Figure 3. Seismic-reflection profiles show variable along-strike changes in Ugak fault scarp height (~4–25 m), which implies different levels of post-Last Glacial Maximum (LGM) fault activity. Clear seafloor offset disappears by MMS 490 (F), which is 25 km SW of sparker profile 242 (E). Profiles are oriented from northwest to southeast (left to right) and shown from northeast to southwest. Note that the vertical and horizontal spatial scales in (A), (B), and (E) (Chirp and sparker reflection lines) differ from (C), (D), and (F) (MMS reflection lines).

travel time. We then compile individual wave fronts from the final model to identify which sources could have shared the same tsunamigenic source location. Note that our approach cannot constrain tsunami wave amplitude and does not consider later arrivals; thus, we do not model near-shore, nonlinear effects on tsunami wave propagation or identify additional tsunamigenic sources associated with later tsunami arrivals. Finally, we compare convergent source locations to identified trench-parallel scarps observed with seafloor topographic data and faults identified with seismic profiling.

The reported first sense of motion for some run-up locations was up, consistent with the Kodiak Islands being located landward of the hanging wall of the Alaska-Aleutian megathrust (Plafker, 1969; Table 1). The one exception was at the northernmost Kodiak City measurement site. Of the seven tsunami sites, five back-projected wave-fields (Kaguyak, Saltery Cove, Cape Chiniak, Kalsin Bay, and Kodiak City) converge ~15 km south of Sitkalidak Island (Fig. 2). Here, we find a conspicuous 50-m-high trench-parallel seafloor scarp that we associate with the KSfz (Fig. 3). Two observations, Kalsin Bay and Old Harbor sites, do not share overlapping wave fronts and arrive too late to be sourced from this region. We note the reported first-arrival time for Old Harbor is inconsistent with this interpretation; it is situated in a sheltered bay (Fig. 2), and a direct tsunami wave from a fault located south of Sitkalidak Island may have experienced a more complex travel path. Thus, all but the measurement from Kalsin Bay is consistent with motion along the fault scarp near Sitkalidak Island (Figs. 2 and 3).

TABLE 1. TSUNAMI TRAVEL TIMES

Inundation site	Travel time (minutes)	Travel-time difference (minutes)	First motion (reported)
Kaguyak	38	6	NA
Old Harbor	48	24	Up
Cape Chiniak	38	0	Up
Kalsin Bay	70	13	NA
Naval Station	63	5	Up
Kodiak City	45	5	Down
Saltery Cove	30	0	NA

Note: Travel-time difference in the third column is taken to be the relative difference in time between the source convergence point (152.715 W, 57.061 N) and the closest distance to each modeled wave front. Modified from Plafker (1969). NA—not applicable.

We infer only part of the KSFz moved in the 1964 earthquake. Had the faults near Kodiak City experienced significant uplift, tsunami wave crests would have arrived sooner to the north (Fig. 2). Similarly, onshore KSfz fault segments did not show evidence for uplift in 1964 (Plafker, 1969; Carver et al., 2008). Thus, measurable uplift related to the GAE was likely limited to a narrow portion of the KSfz near the center of the Kodiak subduction zone segment.

We infer uplift along a short segment of the KSfz during the GAE, where KSfz seafloor lineaments have similar scarp heights along strike (Fig. 3). With scarp heights upwards of 50 m, and an estimated maximum coseismic uplift per event of ~8 m (Plafker, 1969), we conclude that (1) the region surrounding GAE uplift has repeatedly ruptured during Holocene megathrust earthquakes; (2) additional along-strike faults associated with the KSfz have ruptured in a similar fashion during past megathrust earthquakes; and (3) the entire length of this fault should be considered active and tsunamigenic.

Although we show no direct evidence that the ABfz uplifted during the GAE, the convergence of three back-projected travel-time contours from our tsunami analysis lies just beyond the edge of the continental shelf (Fig. 2). Another notable convergence lies at an identified scarp along the ABfz (Fig. 2). Although we favor the KSfz tsunami source, our analysis does not preclude co-rupture or later travel times from other sources. Indeed, assuming horizontal motion from the wedge slope, Suleimani and Freymueller (2020) identified the region near the continental shelf break as a likely tsunami source in 1964. Potential errors in the tabulated travel times (e.g., personal eyewitness accounts and timing) may point to inaccurate back-propagated locations for some of the observations. That being said, we do not see compelling evidence for the GAE first-arrival tsunami source along the ABfz, but we will discuss a scarp and fault that are consistent with postglacial Holocene uplift along the ABfz, closer to the Suleimani and Freymueller (2020) tsunami source region.

KODIAK SHELF FAULTS

To characterize Neogene and younger slip on the KSfz, we present a compilation of vintage and modern active-source seismic profiles that cross seafloor scarps (Fig. 4). Given a 30–50 m up-to-the-north seafloor scarp near our tsunami travel-time convergence region (Fig. 3), and that these KSfz-related scarps presumably developed over the past ~13.5 k.y. (Carver et al., 2008), we infer a long-term uplift rate of 2.2–3.7 mm/yr. If we assume (1) that the faults coseismically slip only during M>8 ruptures, and (2) that they have a recurrence interval of 400 years (i.e., 34 post–Last Glacial Maximum (LGM) earthquakes; Shennan et al., 2018), we would expect 1.4–2.3 m of uplift per M8+ earthquake along this fault. Because our tsunami analysis suggests focused uplift in 1964, the slip-per-earthquake and per-fault must be greater than the long-term average slip to produce multiple pronounced scarps related to the KSfz. Furthermore, the 8 m uplift observed along the Patton Bay fault during the GAE (Plafker, 1969) suggests higher focused uplift is possible, and likely, to produce such fault scarps.

Seismic-Reflection Profiling

Our seismic-reflection data set to characterize the KSfz consists of legacy 24-channel airgun seismic-reflection profiles acquired in 1975 from the former Minerals Management Services (MMS) of Alaska, a sparker seismic profile collected by the MMS in 1976, a Chirp seismic profile acquired in 2018, and a sparker profile acquired in 2015 (Fig. 4). The legacy seismic profiles were obtained as digital scans of stacked travel-time images from MMS permit 75-02 (Liberty, 2013). The 2018 sub-bottom Chirp data were provided to us from the Alaska Amphibious Community Seismic Experiment (Barcheck et al., 2020), and the 2015 sparker data were acquired using a 12-channel, 500-Joule sparker on the U.S. Geological Survey RV *Alaskan Gyre* (Liberty and Ramos, 2016). We migrate and depth-convert the airgun images using stacking velocity values provided with the MMS image scans. We depth-convert the Chirp and sparker data using a velocity of 1500 m/s. We interpret the seismic-reflection data and show faults that offset the seafloor. We begin our analysis with seismic profiles that cross our inferred 1964 tsunami source and then explore profiles northeast and southwest of the tsunami source region.

MMS Line 484

Our back-projection model places the GAE tsunami source location along a northeast-trending scarp close to MMS line 484 within the Kiliuda trough (Fig. 3). Although this seismic profile is low resolution (~35 Hz center frequency or a 40 m predominant wavelength), we note a 3.5-km-wide zone (common depth point [CDP] 145–180) where the seafloor is elevated ~50 m compared to the surrounding regions (Fig. 4). At CDP 140 and CDP 180, we note both truncated and offset reflectors that increase in offset with depth, consistent with fault growth (Fig. 4D). We term the fault at CDP 180 the Ugak fault, because this feature is located offshore of Ugak Island. Based on the proximity to the convergence of tsunami travel-time contours, we interpret coseismic uplift on this fault as the first-arrival source for the 1964 tsunami that inundated several locations on the Kodiak Islands. The seafloor lineation associated with this fault extends at least 80 km (Fig. 3), suggesting that an independent rupture would be capable of generating a M7 earthquake (e.g., Wells and Coppersmith, 1994). We interpret the fault that surfaces near CDP 140 (fault A, Fig. 4D) as a south-dipping back thrust of the Ugak fault that controls the northern margin of the upthrown block. It is also possible that fault A

moved in 1964. The mottled seismic character and rugged seafloor topography within the uplifted seafloor region (CDP 140 to CDP 180) is consistent with deformed Cenozoic strata below the seafloor, similar to that mapped on the Kodiak Islands (Fig. 4D; Moore et al., 1983). The parallel reflectors and smooth seafloor topography to the south of the Ugak fault are consistent with late Quaternary to Holocene marine strata. Here, we interpret a strong-amplitude, seafloor-parallel reflector as the base of modern deposition. Our interpretation is consistent with a regional unconformity that was seismically mapped beneath PWS and the Gulf of Alaska, which likely defines the onset of postglacial sedimentation (i.e., Carlson and Molnia, 1975; Liberty et al., 2013; Finn et al., 2015; Haeussler et al., 2015; Liberty et al., 2019). We observe differentially offset reflectors across the Ugak fault and farther south, suggesting that additional faults near CDP 200 (fault B) and CDP 235 (fault C) have been Neogene-active (Fig. 4D). Although poorly constrained, we estimate a fault dip of 70°–80° for the north-dipping faults. This dip is similar to the near-surface expression of megathrust splay faults mapped near Montague Island (e.g., Plafker, 1969; Liberty et al., 2013, 2019). Using Hayes et al. (2018) Slab2 geometry and assuming simple planar or listric fault geometry, we project the Ugak fault to splay from the megathrust at ~30 km depth beneath the Kodiak Islands.

Faults B and C bound a 2-km-wide anticline and likely converge at about 2–3 km depth (Fig. 4D). The shallowest reflectors do not show measurable offset (upper 100 m below seafloor), suggesting that these faults may no longer be active or measure low slip relative to sediment deposition rates. If the pattern of faulting observed on MMS 484 is characteristic of these fault zones, it may suggest that the majority of Holocene slip is focused on the more landward faults.

Sparker Profile 242

About 5 km to the southwest of MMS 484 and still within the Kiliuda trough (Fig. 3), sparker profile 242 shows the shallow character of the Ugak fault (Fig. 4E). In particular, this higher-resolution view (~1 m dominant wavelength) of the Ugak fault shows a 25 m seafloor scarp toward the northwest (Fig. 4E). Here, we observe no modern deposition in the fault's hanging wall to the northwest (hard water bottom and no sub-bottom reflectivity), an erosion channel directly above the fault, and subparallel reflectors to the southeast of the fault that are consistent with Holocene strata. We observe a second, more moderate seafloor high that we interpret as the hanging wall of fault B (Fig. 4E). While we observe no measurable seafloor offset on MMS 484 across fault B, here we measure a seafloor offset of ~5 m. Assuming these two features both represent fault B, we conclude that either this fault is still active and the legacy airgun profiles do not provide adequate resolution to image Holocene displacements, or the fault slip varies along strike. Although fault C controls the south limb of an anticline on MMS 484, this fault on sparker profile 242 shows little evidence for Holocene motion.

Assuming that the three identified faults along sparker profile 242 represent north-dipping thrust faults, sub-bottom reflectivity suggests sediment deposition is focused on the seaward or footwall side of each fault. At a deposition rate of 1 mm/yr (Carlson and Molnia, 1975), two notable sub-bottom reflectors at ~5 and 10 m below the seafloor are consistent with early and mid-Holocene unconformities; the 10 m reflector represents the Pleistocene–Holocene boundary. Similar age unconformities were inferred from seismic profiles near the PWS region within the Gulf of Alaska (i.e., Liberty et al., 2013; Finn et al., 2015), thus we suggest that these unconformities are pervasive, regionally significant, and with detailed age controls, may be used to compare slip rates across subduction zone segments.

MMS Line 490

The northwest-southeast–oriented MMS 490 is located 60 km to the southwest of MMS 484, outside of the Kiliuda depositional trough (Fig. 3). To explore the southwest extension of active faulting, we trace seafloor scarps and examine the seismic character to identify the Ugak fault at CDP 270, fault B near CDP 345, and fault C near CDP 370 (Fig. 4F). Here, based on reflector offsets, we measure a fault dip of ~65° to the north for the Ugak fault and fault C and ~70° to the north for fault B. We observe that these faults show no measurable offset of reflectors above ~100 m depth, suggesting little Holocene fault motion. Faults B and C define the limbs of a 4-km-wide fold with reflector offsets increasing with depth (Fig. 4F). Small reflector offsets may indicate a back thrust near CDP 200, but the convoluted reflection polarities preclude rigorous interpretation of this portion of the profile. The change in dip angle and reflector character on MMS 490 suggest reduced slip for this portion of the Ugak fault when compared to MMS 484.

MMS Line 480

Along MMS 480, located 20 km northeast of MMS 484, we identify the northeast extension of the Ugak fault as a 30-m-high seafloor scarp with the bathymetry data (Fig. 3). Near CDP 170, we identify the Ugak fault from offset reflectors across a near-vertical fault (Fig. 4B). As with MMS 484 and MMS 490, we identify additional reflector offsets that we relate to faults A, B, and C. MMS 480 lies within the Kiliuda trough, suggesting comparable deposition and/or erosion rates for MMS 484 and 480. We identify the greatest uplift of the Ugak fault closer to MMS 484. As with MMS 484 and MMS 490, MMS 480 shows a 4-km-wide anticline with no measurable seafloor offset (Fig. 4B). Here, this anticline is approximately twice the width when compared to MMS 484, consistent with oblique shortening away from the presumed tsunami source. This fault divergence was also observed near the focus of GAE uplift along the Patton Bay fault system (Liberty et al., 2019), suggesting that more detailed fault mapping is needed to improve our understanding of fault kinematics within the KSfz.

AACSE (Alaska Amphibious Community Seismic Experiment) Chiniak Trough Chirp Profile

Approximately 80 km to the northeast of the Kiliuda trough, we identify another cross-glacial sediment trap termed the Chiniak trough (Fig. 3).

Here, a 3.5 kHz Chirp reflection profile acquired on the RV *Sikuliaq* in 2018 captures a robust postglacial sediment record (Fig. 4A). Along strike of the Ugak fault, we identify a 7.7 m seafloor scarp. Here, we measure a vertical offset of 18 m across a strong amplitude reflector that lies at the base of a package of subparallel reflectors that we presume are related to Holocene deposition (Fig. 4A). From the assumption of a 13.5 ka age basal marker, we estimate an average Holocene deposition rate of ~1.5 mm/yr to the south of the Ugak fault, with a decrease in deposition rate to the north and south away from the fault. Assuming the offset on the interpreted post-LGM surface represents the Holocene slip rate, we estimate an uplift rate of ~1.3 mm/yr. This represents an uplift rate of ~25% of that observed along sparker profile 242 and MMS 484.

BSU Sparker Profile

During 2015, we acquired a 500 J sparker seismic profile with a 12-channel hydrophone array across the northeast extension of the Ugak fault (Fig. 3) (Liberty and Ramos, 2016). This profile, which we term BSU (Boise State University) sparker profile, lies ~20 km to the north of the Chiniak trough sediment trap. Here, the latest bathymetric survey dates back to 1933; therefore, it is unclear from seafloor data alone as to whether tectonic scarps are present. On the BSU sparker profile, our largest seafloor displacement that lies along strike of the KSfz measures 4 m (Fig. 4B). Across this scarp, we measure dipping reflectors in the upper tens of meters that are consistent with Quaternary fault motion. Although we identify no parallel reflectors that would point to Holocene deposition, we identify a reflection pattern that is consistent with some motion on the Ugak fault. With a diminished offset of the seafloor scarp compared to our seismic profiles to the southwest, we suggest that this profile shows where the KSfz becomes less active. We note that trench-perpendicular structures have been mapped to the northeast of this profile location, coincident with the presumed boundary between the Kodiak and Kenai segments (Fig. 1; Fisher, 1980; Fisher and von Huene, 1980).

Summary of Kodiak Shelf Fault Zone (KSfz)

From seismic and bathymetric data, we underscore two points. First, we note a divergence in distance between the Ugak fault and faults mapped to the south, consistent with oblique tectonic shortening along the KSfz. Second, the Ugak fault shows a maximum seafloor displacement along MMS 484 with diminished offset to the northeast and southwest. This may suggest a repeated tsunami source near the Kiliuda trough. Regardless if the Kiliuda trough may be a focus of exhumation, along-strike seafloor scarps point to other tsunami sources that have likely inundated the Kodiak Islands during past earthquakes.

Scarp heights measure higher on the seismic profiles when subparallel faults have separation distances of 5 km or less (Fig. 4). This might suggest that over a 20–30 km along-strike distance, there are changes along the décollement that favor closer splay fault separation and higher uplift rates. MMS 484 shows minor folding northwest of the Ugak fault, whereas reflectors on MMS 490 are relatively undeformed and continuous. Between faults B and C, however, reflectors suggest local shortening and growth faulting. These two faults merge at depth, consistent with a more complex upper-plate structure when compared to a model where faults simply splay from the megathrust

Near Sitkinak Island (Fig. 3), Zimmermann et al. (2019) mapped two linear northwest-side-up scarps that they relate to the KSfz. The northwestern of the two scarps is 20–25 m tall and 29 km long. The southeastern fault scarp, mapped only with single-beam bathymetry, may be upwards of 45 m tall and 80 km long. These observations imply that although the Ugak fault diminishes to the southwest, as mapped by MMS 490, the KSfz consists of many tsunamigenic faults whose interactions are poorly understood or constrained. This pattern differs from that observed along the offshore PWS faults, where a more focused exhumation region is observed (Haeussler et al., 2015; Liberty et al., 2019).

In summary, we find the ~200-km-long KSfz contains variable scarp heights and along-strike variation in faulting style, although it is a long and laterally continuous structure. Large changes in seafloor scarp height and evidence for tsunami generation along the fault zone in 1964 argue for repeated, discrete KSfz uplift during megathrust slip, which translates to a high tsunamigenic fault hazard at distances close to populated areas. We presume that the KSfz splays from the megathrust near the southeastern limits of the Kodiak Islands. Coupled with onshore faults that indicate sinistral slip (e.g., Carver et al., 2008), the KSfz is a complex contractional fault system, which is possibly transpressional. Our observations warrant additional paleoseismic investigations. More detailed bathymetric and seismic mapping is needed to fully characterize the fault slip, interaction with the megathrust, and seismic hazard for this fault system.

■ ALBATROSS BANKS FAULT ZONE

From the low-resolution, 24 arc-second bathymetry data set, we do not identify seafloor scarps near the shelf break that are similar in magnitude and length to the KSfz (Fig. 5). The few multi-beam tracks that pass through this area point to a single seafloor uplift that we explore here. Our initial bathymetric assessment, coupled with seismic results of Fisher (1980) and Fisher and von Huene (1980) is consistent with (1) a majority of Holocene fault motion, as observed on the seafloor, being accommodated around the KSfz and (2) that the currently available low-resolution bathymetry cannot capture the full seafloor expression of the ABfz. In other words, there are likely other seafloor scarps along the ABfz that we have yet to identify. These possibilities are examined in greater detail with seismic profiles.

Great Alaska Earthquake (GAE) Tsunami Source

We begin our discussion of the ABfz in the vicinity of a prominent fault scarp that we identify on MMS 464 and the coincident BSU sparker seismic profile (Figs. 5 and 6). This location is consistent with tsunami travel times from Kodiak City and Cape Chiniak (Fig. 2). Had this location solely sourced a tsunami, Plafker (1969) would have measured an earlier arrival

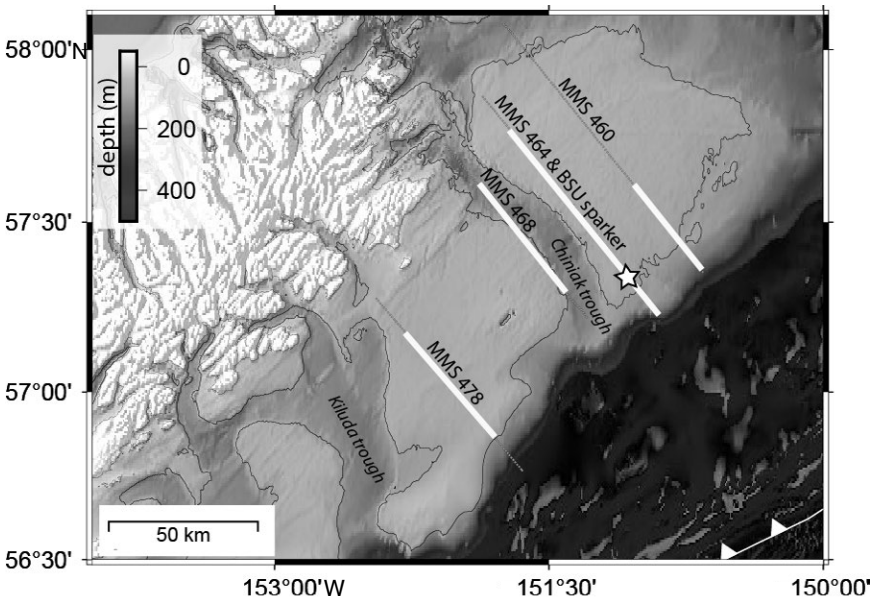

Figure 5. 24-arc second bathymetry across the Kodiak shelf detailing the Albatross Banks region and select Minerals Management Service (MMS) seismic profiles. Portions of the seismic profiles highlighted on Figure 6 are shown in white. The star represents a 16-m-tall scarp identified with MMS line 464 airgun and BSU sparker profiles. This is a possible tsunami source, consistent with Kodiak City and Cape Chiniak tsunami travel times.

time from the Kalsin Bay station and later arrival times from the other stations farther to the southwest (Table 1). Given two tsunami sources, one from the Ugak fault and one from this scarp, Plafker (1969) would have still observed an earlier travel time from the Kalsin Bay station (Fig. 2). Thus, assuming accurate tsunami arrival times, we conclude that the fault that lies beneath this scarp did not produce tsunamigenic uplift during the GAE. It is possible that the shelf slope region identified by Suleimani and Freymueller (2020) did produce a tsunami, but travel times from this location would have arrived later on all stations than what Plafker (1969) documented.

MMS Line 464 and BSU Sparker Profile

MMS 464 and the BSU sparker profile are coincident, lie immediately east of the Chiniak trough, and both cross the KSfz and ABfz (Fig. 5). Where these profiles cross the ABfz, we measure about a 16 m seafloor scarp (Figs. 6B and 6C). This scarp lies above a monocline that is consistent with the upper-plate expression of a megathrust splay fault (e.g., Liberty et al., 2013; Fig. 6C). We estimate a fault dip of ~80° on the shallow portion of this fault. The BSU sparker seismic profile shows south-dipping strata and reflector truncations beneath the scarp (Fig. 6B). Given the seismic character and location on the shallow shelf, we interpret the shallow stratigraphy as representing pre-Holocene strata. Thus, a robust Holocene slip-rate estimate was not possible for this fault at this location. However, with the assumption that seafloor topography was reset during the LGM, this fault has likely been active during many Holocene earthquakes. Thus, we interpret this scarp as tsunamigenic. If the 16 m scarp developed only over the past 13.5 k.y., we estimate a slip rate of 1.2 mm/year.

MMS Line 460

MMS 460 is located near the transition from the Kenai to Kodiak segment, 20 km to the northeast of MMS 464 (Figs. 1 and 5). The seismic profile shows asymmetric, km-scale folding bound by three faults between CDP 640 and 725 (Fig. 6A). The distance between each ~70° SE dipping fault is less than 5 km, and offset reflectors cannot be traced to the seafloor, implying relatively low Holocene slip rates. It is unclear how each of these faults relates to the presumed tsunamigenic fault highlighted on MMS 464, but the changing seismic character over a length scale of 20 km suggests that the ABfz is complex. The lack of a seafloor scarp suggests limited Holocene motion near the Kenai segment boundary.

MMS Line 468

MMS profile 468, located 20 km to the southwest of MMS 464, crosses the Albatross Banks near the Chiniak trough (Fig. 5). On this profile, we identify a single high-angle splay fault near CDP 685, which lies along strike of the tsunamigenic fault identified on MMS 464 (Fig. 6D). There is noticeable folding on the hanging-wall side of this presumed splay fault to less than 300 m below the seafloor. The fault does not appear to offset the seafloor. This suggests that the tsunamigenic seafloor scarp is not regionally extensive and that focused uplift is restricted to a narrow region surrounding MMS 464.

MMS Line 478

MMS 478 lies between the Chiniak and Kiliuda troughs (Fig. 5). We note a prominent anticline centered near CDP 440, the axis of which trends northwest-southeast (Fisher and von Huene, 1980; Fig. 6E). On this profile, we identify two high-angle splay faults that are separated by ~7 km. Folding is tighter across the northwest fault's hanging wall (CDP 400) compared to the hanging wall of the fault at CDP 460 (Fig. 6E). We observe no shallow offset stratigraphy across either fault, suggesting little to no Holocene motion.

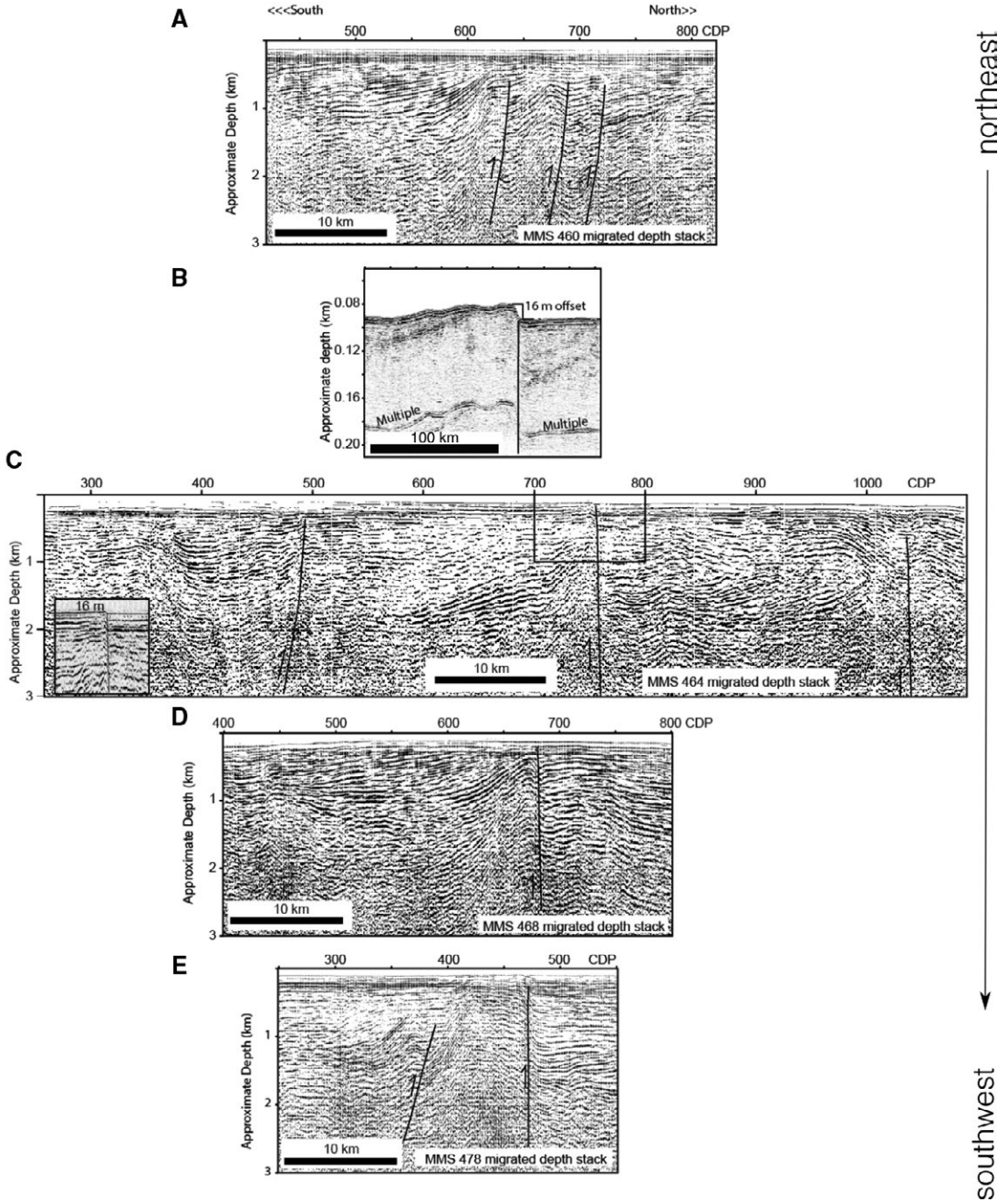

Figure 6. Minerals Management Service (MMS) airgun and sparker seismic-reflection profiles of the Albatross Banks fault zone (ABfz). (A), (B), (D), and (E) show prominent splay faults that bound forearc basin structures but do not appear to offset the seafloor. (B) In contrast, shows an ~16-m-high fault scarp that we imaged in 2015 with a sparker seismic source. We infer a Holocene slip rate of 1.2 mm/yr for this particular fault.

Summary of Albatross Banks Fault Zone (ABfz)

Faults belonging to the ABfz are largely reverse faults originally mapped offshore Kodiak between Sitkinak Island to the southwest and the Kenai segment boundary to the northeast (von Huene et al., 1980; Figs. 1 and 3). However, its near-surface architecture, Holocene activity, and along-strike extent are largely unknown. Limited and generally low-resolution bathymetry data for this region do not show conspicuous seafloor lineaments that we could interpret as Holocene fault scarps (Figs. 2 and 3). But the seismic data allowed us to identify a 16 m scarp that suggests recent tectonic activity. The MMS airgun seismic data do not have the resolution to image seafloor offsets less than ~10 m, and this underscores the need to use both high-resolution bathymetry and sparker seismic data together to interpret fault activity.

A Comparison of Kodiak Shelf Fault Zone (KSfz) and Albatross Banks Fault Zone (ABfz)

Although our data sets are limited, we find that both the scarp height and morphology associated with the KSfz are much more prominent than those associated with the ABfz. Such an observation implies a majority of Holocene faulting has been accommodated closer to the Kodiak Islands shoreline (i.e., KSfz) rather than along faults nearer to the edge of the shelf (i.e., ABfz). An increase in fault scarp height may indicate that through time, the location of focused deformation transitioned from the outer to inner wedge regions of the forearc, which is expressed in the higher uplift rates of the KSfz compared to the rates for the ABfz that we infer. One plausible hypothesis is that higher splay fault activity (exhumation) is a function of where the wedge changes from mechanically weak (outer wedge) to strong (inner wedge backstop). In the PWS region, thermochronology and seismic-reflection data show that a major splay fault separates these regions (Liberty et al., 2013; Haeussler et al., 2015). Rocks accreted before and after the subduction of a spreading center in the Gulf of Alaska are similar in age between PWS and those onshore of the Kodiak Islands (Bradley et al., 2003). Different accretionary episodes form the strong-to-weak wedge transition, and the location of the KSfz roughly coincides with this structural boundary. Alternatively, the deformation rates have always been higher within the KSfz than the ABfz, which is still consistent with differences in wedge mechanical strength. We conclude that the tsunamigenic fault hazard is concentrated in the near-shore region of the Kodiak Island, although the ABfz and slope regions are still capable of producing tsunamis.

UPPER-PLATE AND PLATE BOUNDARY STRUCTURE

Gravity and magnetic data can reveal unique signals of subducting and upper-plate structure. Despite the numerous studies that have uncovered correlations between moment release, subducting structure, and down-dip rupture limits (e.g., Song and Simons, 2003; Wells et al., 2003; Bassett and Watts, 2015), the Alaska subduction zone in particular seems to be more complex for understanding seismogenic behavior. A positive gravity anomaly dominates the Alaska forearc (Fig. 7A), and this anomaly was interpreted by Wells et al. (2003) as resulting from a highly dense inner-wedge or duplexed structure near the plate interface. Seamounts and fracture zones on the Pacific plate offshore Kodiak are observed on gravity and magnetic data, but subducted expressions of these structures below the forearc are lacking (Saltus et al., 2007; von Huene et al., 1999; Mankhemthong et al., 2013; Figs. 7A and 7B). Thus, the relationship between coseismic rupture, subducted topography, and upper-plate splay faulting deserves further scrutiny for the Kodiak Islands region.

Gravity Data

Free-air gravity anomalies over subduction zones map density differences related to either plate interface or upper-plate structures (Smith and Sandwell, 1997). The spatial distribution of the free-air gravity field over the North American and Pacific plates near the Kodiak Islands shows several regional tectonic features that may influence seismogenesis (Wells et al., 2003; Bassett and Watts, 2015). We apply upward-continuation and bandpass filtering to the free-air gravity field to constrain the extent and geometry of the accretionary prism and upper-crustal faulting (Figs. 7 and 8).

The free-air gravity map of the Kodiak-Kenai Peninsula region helps to clarify relationships between rock units in the accretionary prism. The Border Ranges fault zone marks the contact between the Mesozoic and Cenozoic accretionary prism and its backstop (Fisher, 1980; Plafker and Berg, 1994; Pavlis and Roeske, 2007; Mankhemthong et al., 2013). This fault coincides with a conspicuous gravity lineament that bounds the northwest extent of the Kodiak Islands (Fig. 7A). To the southeast of the Kodiak Islands, a northwest to southeast transition from low to high gravity signals forms a lineation that defines the boundary between the older "Chugach terrane" part of the accretionary prism and the younger Paleocene–Eocene "Prince William terrane" (Burns et al., 1991; Plafker et al., 1994; Wells et al., 2003). These two terranes are considered to divide the accretionary complex (Plafker et al., 1994), but the upper plate across this boundary consists of no discernable density contrast. Instead, this anomaly has been interpreted to stem from duplexing or other crustal densification processes near the plate boundary (Wells et al., 2003; Mankhemthong et al., 2013). In addition, significant rock uplift of the accretionary complex has brought higher velocity and presumably denser rocks closer to the surface. This regional exhumation process might also explain the source of the positive gravity anomaly (Ye et al., 1997) that may structurally link the KSfz and Patton Bay fault systems (Figs. 7 and 8). Of note is that the related gravity lineation extends across segment boundaries where seafloor scarps and active faults have not been mapped.

We observe two circular gravity lows that bound the Kodiak Islands to the northeast and southwest, which were first noted by Wells et al. (2003) (Fig. 7). These ~120-km-wide low-gravity regions lie between the Border Ranges fault zone to the north and the Prince William terrane boundary to the south. The limits of these gravity lows also coincide with our

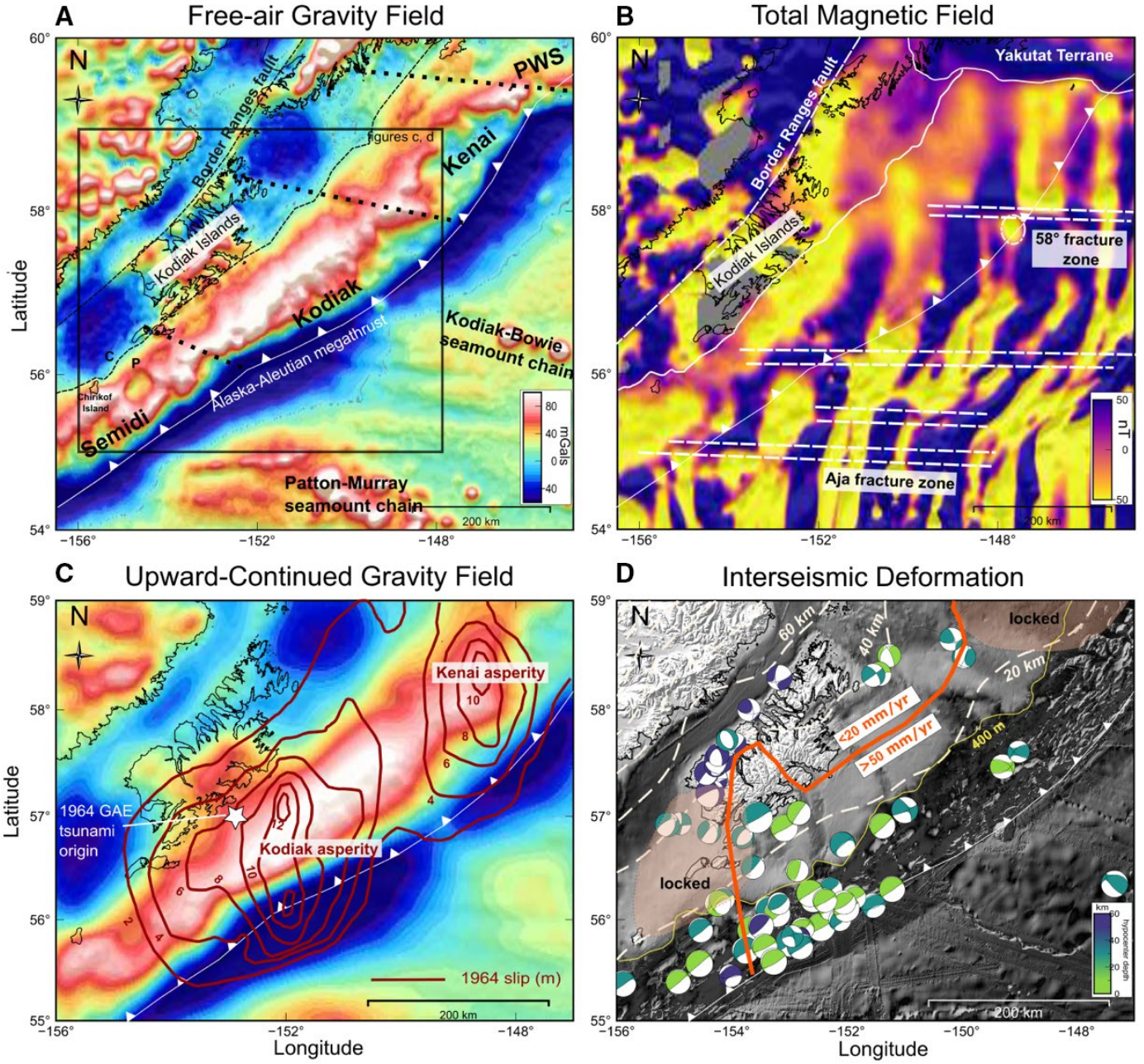

Figure 7. Geophysical expressions of crustal structure and segmentation across the western Gulf of Alaska. (A) Free-air gravity anomaly map (Sandwell et al., 2014). Dotted black lines signify segment boundaries discussed in the text. Dashed black lines denote Border Ranges fault. Box denotes location of (C) and (D). (B) Total magnetic field from the EMAG2 database (Meyer et al., 2017). Gray regions represent data gaps. Solid white lines signify terrane boundaries. Major fracture zones (dashed white lines) from Naugler and Wageman (1973) are revealed as offset magnetic lineations. Note that several fracture zones (e.g., 58 °fracture zone, Aja fracture zone) appear landward of the trench. (C) Upward-continued free-air gravity anomaly to a height of 10 km. Superposed are coseismic 1964 slip contours (2 m) of Ichinose et al. (2007). We observe that slip was confined mostly to the positive gravity anomaly regions. (D) Seafloor bathymetry map with post-1964 earthquakes (M>5) colored by hypocenter depth and plate-locking model from Zweck et al. (2002). The 400 m bathymetry contour (yellow) delimits the continental shelf break. The bold orange line signifies a major change in the slip-rate deficit as derived from geodetic inversion analysis (Li et al., 2016). Focal mechanisms from the CMT catalog (1976–2016) show the along-strike contrast in interseismic stress release following the Great Alaska Earthquake (GAE) for the Kodiak region. Off-white dashed lines show the depth to the plate interface in 20 km intervals from the Slab2 model (Hayes et al., 2018).

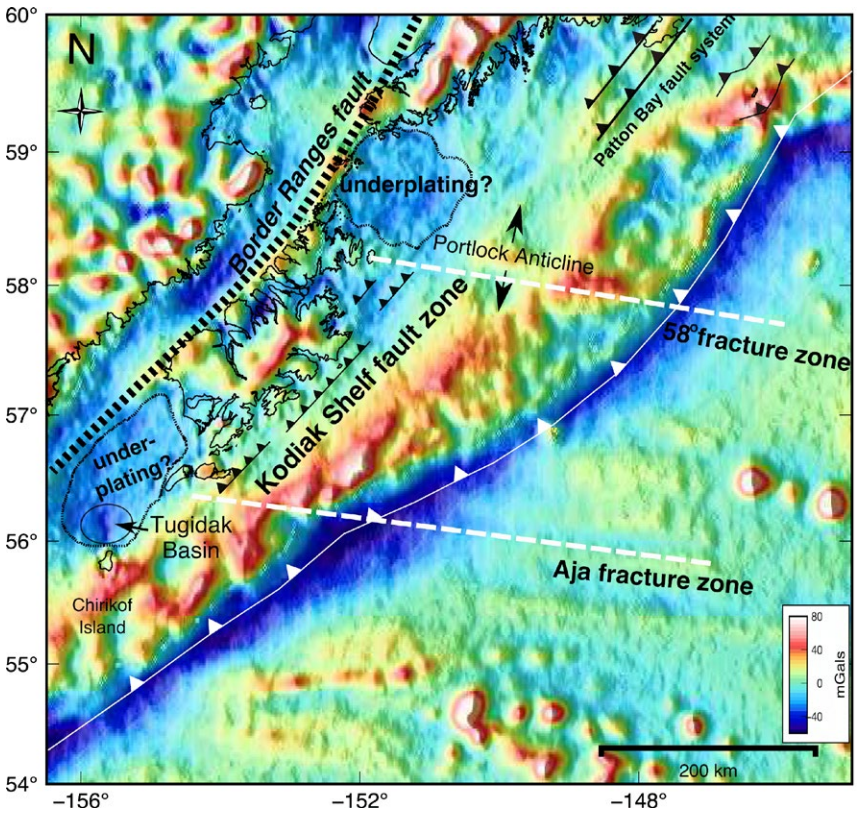

Figure 8. Low-pass filtered free-air gravity map for the Gulf of Alaska region. This map is filtered to remove signals with wavelengths greater than 100 km and illuminated from the southeast to highlight gravity lineaments related to forearc splay faults and terrane boundaries. Note the continuity of the Kodiak Shelf fault zone (KSfz) and its gravity expression diminishes seaward of the Alaska forearc. Splay faults belonging to the Patton Bay fault system are also highlighted farther to the north on the Prince William Sound (PWS) segment. The gravity signature of the subducted 58°N fracture zone within the wedge and its upper-plate structural expression (Portlock Anticline) share the same N85W oblique trend. Two prominent low-gravity anomalies south and north of the Kodiak Islands are interpreted as possible sites of underplating. Note these two gravity lows bound both the mapped KSfz and the projection of subducted 58°N and Aja fracture zones (white dashed lines).

mapped extent of the KSfz (von Huene et al., 1980). The observed correlation between positive gravity anomalies and active splay faults suggests that offshore faults within the Prince William terrane (i.e., KSfz and ABfz) may have higher slip rates compared to faults closer to mainland Alaska.

Ye et al. (1997) identified a low seismic velocity mid-crustal body that spatially matches the large northern gravity low between the Kodiak Islands and Kenai Peninsula. This gravity and/or seismic velocity low could be evidence for large-scale underplating of subducted sediment or a seamount as proposed by Ye et al. (1997) and Mankhemthong et al. (2013). The oblate negative gravity anomaly to the southwest of the Kodiak Islands does not correlate with any previously suggested upper-plate (mid- to lower-crustal) source (Figs. 7 and 8). The upper Miocene to Quaternary Tugidak basin has been mapped on Chirikof and part of the Trinity Islands, but this shallow basin may not account for the observed gravity low. Similar to the gravity anomaly that bounds the northeast side of the Kodiak Islands, we hypothesize that lower crustal underplating may be the source of this anomaly, because this feature persists even on the filtered long-wavelength component of the free-air gravity field (Fig. 8).

Our examination of the gravity data does not further constrain this interpretation; however, the spatial relationship between these two gravity lows that sandwich the high elevation Kodiak Islands may link underplated regions to lower exhumation rates. Moreover, the northeastern gravity low appears to correlate with our current understanding of subduction zone segmentation, and it correlates with a region of high slip-rate deficit outlined by Li et al. (2016) (Figs. 7 and 8).

Farther southwest along the Semidi segment, the negative gravity anomaly becomes positive (Wells et al., 2003). This observation indicates a different crustal character between subduction zone segments. Few crustal seismic-reflection data exist across this region (e.g., Bécel et al., 2017). Robust forward potential field modeling of additional crustal-scale seismic-reflection data may be needed to assess underplating as a possible tectonic mechanism. If underplating is occurring both northeast and southwest of the Kodiak Islands, this stresses the importance of interface processes controlling splay fault activation and megathrust segmentation.

Magnetic Data

The total-magnetic field around the Kodiak Islands highlights several distinct tectonic structures on the upper plate and topography on the incoming Pacific plate (Fig. 7B). Some of these continuous or offset magnetic lineations correspond to inferred earthquake segment boundaries (von Huene et al., 1999; von Huene et al., 2012). In particular, the total magnetic field shows offsets of the oceanic-plate magnetic stripes that are most likely sourced by fracture zones (Naugler and Wageman, 1973). The

pattern of magnetic stripes is continuous across the trench, showing that incoming plate structures are imaged below the accretionary wedge and outer forearc (Fig. 7B). Offset magnetic lineations on the incoming Pacific plate reveal at least four main fracture zones that are presently subducting near, and beneath, the Kodiak Islands. The Aja and two unnamed fracture zones are observed south of 57°N latitude. A magnetic lineation related to the 58°N fracture zone persists almost to 200 km northwestward of the trench, down to a plate interface depth of ~20 km (Hayes et al, 2018). This lineation lies at the inferred northeast boundary of the Kodiak subduction zone segment (von Huene et al., 1999; von Huene et al., 2012; Shennan et al., 2014). We note that although the KSfz lies between the landward extension of the 58°N and Aja fracture zones, these features have presumably migrated northwest with plate motions, and there may be no relationship with the lateral extent of the KSFz (Fig. 7).

Both the Chugach and Prince William terrane boundary (seaward of the Kodiak Islands) are revealed by magnetic field gradients, where the total-field switches from positive to negative (Fig. 7B). We consider magnetic anomalies to be features in the total magnetic field data that disrupt the otherwise contiguous nature of upper-plate magnetic signatures. A majority of both the Chugach and Prince William terranes are characterized by negative total-field magnetic anomalies, as expected of accreted sediments that contain little to no magnetically susceptible minerals (Blakely, 1996; Saltus et al., 2007). Furthermore, this negative magnetic anomaly is clearly bound by the Border Ranges fault system to the northwest; the northern region of the magnetic domain of the Border Ranges fault has been referred to as the "Knik Arm" anomaly (Grantz et al., 1963). In the northern Gulf of Alaska, the southern limit of the Yakutat terrane is highlighted by a linear magnetic high anomaly that also coincides with the presumed southwestern PWS segment boundary asperity (Bruns, 1983; Brocher et al., 1994). The major magnetic domains evident on the upper plate are the southern Alaska magnetic high and the Chugach magnetic low, which are sourced from dense lower-crustal mafic and upper-crustal sedimentary rocks, respectively (Saltus et al., 2007).

RELATIONSHIPS BETWEEN FAULTING, SUBDUCTING STRUCTURE, AND LOWER-CRUSTAL DEFORMATION

In order to relate structural controls of segmentation and subducting plate influences to upper-plate deformation across the Kodiak region, we compare 1964 earthquake slip models to potential field and post-1964 seismicity and geodesy data (Fig. 7C). Coseismic models from the 1964 earthquake reveal three main slip patches, or asperities, from joint inversions of geodetic, seismic, and tsunami data (Johnson et al., 1996; Ichinose et al., 2007). The southwestern, or Kodiak asperity, with 10–12 m slip, was focused below the shallow forearc with down-dip rupture generally not extending across the Prince William terrane boundary (Ichinose et al., 2007). The second asperity lies offshore the Kenai Peninsula and northeast of the Kodiak Islands (von Huene et al., 1980; Ichinose et al., 2007). We refer to this ~100-km-wide slip concentration as the Kenai asperity (Cohen and Freymueller, 2004; Kelsey et al., 2015). When we upward continue the free-air gravity field to a height of 10 km, the resultant low-pass gravity field shows that the high-slip regions of both the Kodiak and Kenai asperities are within the positive gravity region (Fig. 7C). We note that this particular slip inversion had limited azimuthal seismic station coverage, and inversion resolution is dependent upon three different data sets (Ichinose et al., 2007). In general, forearc basin depocenters (negative gravity anomalies) correlate with asperity location (e.g., Song and Simons, 2003; Wells et al., 2003); however, here it does not, as previously noted for the Alaska-Aleutian subduction zone by Wells et al. (2003) and Ichinose et al. (2007).

The 58°N fracture zone divides the 1964 GAE slip maxima of the Kodiak and Kenai asperity boundaries (Figs. 7B and 7C). If this fracture zone is indeed a persistent segment boundary, the 1964 earthquake either had enough energy to rupture across the 58°N fracture zone, or perhaps the fracture zone only halted rupture momentarily, as has been observed in the M8.4 Peru megathrust earthquake in 2001 (e.g., Robinson and Watts, 2006). Moreover, paleoseismic evidence indicates the Kodiak asperity sometimes ruptures with, or sometimes independently of, the Prince William Sound asperity (Shennan et al., 2014). Geodetic models show spatial distributions of interseismic locking are different from coseismic strain release (Zweck et al., 2002; Suito and Freymueller, 2009; Li et al., 2016). The 58°N fracture zone does not show a strong gravity signal on the incoming Pacific plate, which is likely due to 2–3 km of low-density sediment subducting beneath the trench (Reece et al., 2011; von Huene et al., 2012; Gulick et al., 2015; Fig. 7A). The E-W magnetic lineament traces the 58°N fracture zone beneath the Pacific plate, and an oblique N85°W-trending (filtered) gravity anomaly coincides with this feature beneath the wedge (Fig. 8). The gravity field records differences in density due to structural juxtapositions in upper-plate deformation, which is probably driven by oblique convergence of the subducting Pacific plate. Fracture zone morphology is typified by a large ridge and trough structure that remains structurally competent as it spreads from the mid-ocean ridge and into the subduction zone (Menard and Atwater, 1969; Sandwell, 1984). The outer wedge of subduction zones is the mechanically weaker portion of the subduction zone forearc (Wang and Hu, 2006;). Wedges thus record recent and current deformation of subducting high relief from the incoming plate, such as seamounts or fracture zones (Basset and Watts, 2015). Considering both fracture zone morphology and constraints from both potential field data sets, we interpret the N85°W-trending feature to be the upper-plate expression of the subducted 58°N fracture zone below the outer wedge. Furthermore, a concentric anomaly in the total magnetic field near the trench suggests a subducted seamount may be associated with the 58°N fracture zone (Fig. 7B; Fruehn et al., 1999; von Huene et al., 2012).

The Kodiak segment transitions from strongly to moderately locked below the Trinity Islands and northeast of the Kodiak Islands (Fig. 7D). This is in contrast to that observed with the PWS segment, which is completely locked (Zweck et al., 2002; Sauber et al., 2006; Freymueller et al., 2008). The abrupt low-to-high change in the gravity field between the Tugidak basin and the Kodiak Islands suggests a potential field signature of this rupture boundary (Fig. 7A). Moreover, lower-plate conditions change along the Gulf of Alaska from PWS to the Kodiak

Islands. For instance, the trailing edge of the Yakutat terrane (Fig. 7B) is highly coupled to the Pacific plate (Brocher et al., 1994; Zweck et al., 2002). These structures together have much shallower dip (~4°) when compared to the Kodiak region, where the dip gradually steepens to ~10° (Brocher et al., 1994; Eberhart-Phillips et al., 2006; Sauber et al., 2006; Hayes et al., 2018). Roughness of the subducting Pacific plate could also influence regional variations in coupling because there are numerous seamounts and fracture zones sitting offshore from the Kodiak Islands, as shown in the potential field data.

Post-1964 seismicity varies along-strike across the Kodiak Islands (Fig. 7D). There is a relative paucity of large earthquakes (M>5) for the northeast region, and a majority of the seismicity is occurring offshore and southwest of the Kodiak Islands, suggested by others to have occurred in the subducting Pacific plate (Doser et al., 2002; Doser, 2005). Focal mechanisms in the southwest Kodiak region are consistent with thrust faulting where the hypocenters cluster between 20 and 40 km depth. Models suggest the megathrust is mostly locked landward of these moderate seismic events (Zweck et al., 2002). However, shallow thrust events coupled with significant margin erosion, which may cause a shallowing of the slope angle, suggest that the southwest region of Kodiak may be in the under-thrusting phase of the accretionary cycle (Gutscher et al., 1998). Under thrusting focused beneath the shelf may be accommodating some interseismic slip and may provide a means to maintain down-dip locking below southwest Kodiak. A lack of under thrusting near the plate interface may also explain why the KSfz tapers out across the Semidi segment.

Semidi/Kodiak Segment Boundary

Rupture models for a 1788 A.D., a 1440–1620 A.D., and a 1060–1110 A.D. earthquake recognize a semi-persistent boundary near the Trinity Islands (Briggs et al., 2014; Shennan et al., 2014; Kelsey et al., 2015; Fig. 3). The oblique subduction of fracture zones and seamount chains could complicate megathrust interface conditions and upper-plate deformation, and could exert enough structural control to act as a segment boundary (von Huene et al., 2012). A pronounced gravity gradient parallels the KSfz. This lineament extends southwest of Chirikof Island and northeast to the Portlock anticline (Figs. 7 and 8). The gravity signature related to the KSfz terminates near the northern segment boundary, but a similar gravity signature does not define the Kodiak/Semidi segment transition. The related lineation may instead mark the location of the eroding continental shelf-break, or alternatively, could represent older splay faults that do not offset the seafloor.

Observations from multi-channel seismic-reflection data (ALEUT experiment) across the Semidi and Shumagin segments suggest that the hydration state of the megathrust and structure of the incoming plate play pivotal roles in regulating seismicity and fault formation (i.e., Shillington et al., 2015; Li et al., 2018). Intermediate-depth earthquakes are more abundant across the Shumagin and Kodiak regions, suggesting the Semidi segment is in a different stage of the earthquake cycle (Shillington et al., 2015). In addition, these earthquakes may be below the continental Moho, but ray coverage is insufficient to image deeper megathrust structure in detail (Bécel et al., 2017). Regarding upper-plate structure, the central Semidi segment appears to have several high-angle splay faults within the outer wedge, seaward of the continental shelf break (Li et al., 2018). However, splay faults landward of the continental shelf break are largely unknown on the Semidi segment (von Huene et al., 1987; von Huene et al., 2012). Preexisting structural heterogeneity on the incoming plate can permit fluids to enter the subduction zone and increase the pore pressure, thereby reducing the effective normal stress and making it easier for earthquake rupture to propagate through this region, once initiated. This mechanism is inferred to be responsible for the greater number of intermediate-depth earthquakes for the Shumagin and Kodiak segments (Shillington et al., 2015). Our results agree with this interpretation for the southwest Kodiak segment, especially because offset magnetic lineations in the oceanic crust (corresponding to fracture zones), when subducted at the trench, could contribute to fault-bending and be favorable to fluid permeation (Fig. 7B).

Kodiak/Kenai Segment Boundary

The northeastern boundary of the Kodiak segment has been inferred to exist somewhere between the northern Kodiak Islands and the Kenai Peninsula (e.g., von Huene et al., 2012). Although Johnson et al. (1996) and Ichinose et al. (2007) show an isolated 1964 slip patch between the PWS and Kodiak segments, only recently have geologic observations been made that suggest an independent Kenai segment (e.g., Hutchinson and Crowell, 2007; Shennan et al., 2014; Kelsey et al., 2015). If so, then it seems likely that there is some structural expression of the segment boundary between the Kodiak Islands and the Kenai Peninsula.

We have newly characterized the 58°N fracture with magnetic and gravity data (Figs. 7 and 8). A prominent structural high on the upper plate lies immediately above the subducted 58°N fracture zone on the Kodiak forearc and sources the positive gravity lineament on the landward side of the continental shelf break (Fig. 7; Fisher, 1980). The trend of both the related anticline and this fracture zone bound the negative gravity anomaly to the north of Kodiak Islands (Figs. 7A and 8). However, the uplift is Miocene to Pliocene in age (von Huene et al., 1987) and is most likely not associated with subduction of the 58°N fracture zone because the depth to the plate interface is nearly 20–25 km below the anticline (Hayes et al., 2018). Northwest of the 58°N fracture zone trend, however, KSfz scarp heights diminish and offset reflectors in MMS reflection profiles do not extend to the seafloor. KSfz scarps are not apparent onto the Kenai segment, which suggests the zone of focused uplift (i.e., active splay faulting) does not persist onto the negative gravity anomaly region (Fig. 7A). Unfortunately, geodetic inversions lack resolution across the Kodiak/Kenai segment transition, because it lies sufficiently far offshore (Zweck et al., 2002; Freymueller et al., 2008; Li et al., 2016). The Ichinose et al. (2007) slip model shows that the middle asperity is confined to the Kenai Peninsula region, and the 58°N fracture zone forms a possible southern boundary (Fig. 7C); though the influence of a subducted fracture zone is speculative. Thus, there is a structural (KSfz), geophysical (gravity and magnetics), and coseismic expression

(slip model) of physical property changes that can be related to inferred plate interface conditions.

The Kodiak and Kenai segment boundary may also be driven by differences in subducting sediment volume. Between the 58°N fracture zone and PWS, there is an absence of significant structural relief on the incoming plate, and sediment from the Surveyor Fan is the primary material above the oceanic crust (Reece et al., 2011). Seismic-reflection profiles show >1 km of sediment near the trench (Fruehn et al., 1999). Assuming enough of the Surveyor Fan has been subducted, this sediment may contribute to the low-velocity anomaly, negative free-air gravity, and general lack of thrust earthquakes occurring near the interface below the Kenai Peninsula (Ye et al., 1997; Doser et al., 2002). Furthermore, geomechanical models of forearc basin growth and wedge dynamics show that if there is significant sedimentation on the upper plate, then pervasive internal deformation (i.e., faulting) in the forearc basin is not favored because the wedge becomes stable due to lower shear traction on the megathrust (Fuller et al., 2006).

Porto and Fitzenz (2016) adopted a Bayesian approach using earthquake catalog data to assess segment boundaries for the Alaska subduction zone. Their methodology suggests a potential segment boundary northeast of the Kodiak Islands. This is broadly consistent with the along-strike change in focal mechanism character (i.e., Fig. 7D) and where we interpret the northeast termination of the KSfz.

FAULT SEGMENT SUMMARY

We infer from legacy seismic-reflection data (MMS profiles) that the KSfz faults are splay faults that diverge from, or near, the megathrust at ~30 km depth. This depth is greater than the 20 km depth of the plate interface beneath splay faults in the PWS region (Brocher et al., 1994; Liberty et al., 2013; Haeussler et al., 2015); however, this is likely due to simple Pacific plate subduction below the Kodiak region compared to the additional Yakutat terrane subduction near PWS (Moore et al., 1991; Ye et al., 1997). Focused uplift along the KSfz near the Kodiak Islands shoreline exceeds that of the ABfz in the along-dip direction of the megathrust and is limited in the along-strike direction by the region of under thrusting to the southwest and subduction of the 58°N fracture zone to the northeast. Wells et al. (2003) inferred that crustal duplexing might be the source of the unique gravity signal across the Kodiak Islands. Previous studies near PWS find that splay faulting is assisted by crustal duplexing above the megathrust (i.e., Liberty et al., 2013, 2019; Haeussler et al., 2015). Megathrust duplexing is one hypothesis supporting the observed Kodiak Islands gravity character and uplift patterns of the KSfz. We do not have complementary constraints on megathrust geometry at depths greater than 10 km across the central Kodiak Islands, but the Slab2 model (Hayes et al., 2018) would place the region of duplexing near 25 km depth to the plate interface.

CONCLUSIONS

We identify and characterize upper-plate splay fault uplift patterns that may be driven by plate interface conditions. The active faults that we identify have persisted across the Kodiak Islands offshore region during many Holocene megathrust earthquakes. Subduction of fracture zones, seamounts, and sediments may drive megathrust segmentation and delimit where active splay faults are found along the Gulf of Alaska margin.

A near-shore tsunami risk is present for coastal populations on mainland Kodiak Island. Our tsunami modeling offers an updated view on how tsunamigenic faults uplift in response to megathrust slip offshore of the Kodiak Islands. We find that a narrow region of the Kodiak Shelf fault zone is consistent with the tsunami source during the GAE because a majority of propagated wave fronts converge to one location where we image tall fault scarps (>20 m). We term this tsunamigenic fault the Ugak fault. This fault, and parallel faults of the KSfz, should be included in seismic and tsunami hazard analysis of the region.

Overall, the spatial variability in the KSfz seafloor scarp height indicates discrete, short (<30 km) uplift patterns, and thus fault segmentation. More detailed, high-resolution bathymetric and seismic-reflection data would help to further constrain fault characteristics and slip rates, especially near proposed segment boundaries.

DATA AND RESOURCES

For our tsunami source and fault mapping analysis, we utilize a regional bathymetry data set to identify Kodiak shelf seafloor scarps (NOAA National Geophysical Data Center, 2009, Southern Alaska Coastal Relief Model: NOAA National Centers for Environmental Information: https://doi.org/10.7289/V58G8HMQ). Seafloor topographic data are available from NOAA at https://www.ngdc.noaa.gov/mgg/bathymetry/hydro.html. The legacy seismic profiles were obtained as digital scans of stacked travel-time images from MMS permit 75-02 (https://www.boem.gov/Geological-and-Geophysical-Data-Acquisition-and-Analysis/; Liberty, 2013). EMAG2: Earth Magnetic Anomaly Grid (Maus, 2009) was obtained from the NOAA National Centers for Environmental Information. Global marine gravity model from CryoSat-2 and Jason-1 was obtained from the National Geophysical Data Center at https://data.noaa.gov (Sandwell et al., 2014).

ACKNOWLEDGMENTS

We thank the Associate Editor Craig H. Jones and two anonymous reviewers for their constructive evaluation of this paper. We also thank R/V *Alaska Gyre* Captain Greg Snegden for his help with the 2015 marine seismic data acquisition and acknowledge the careful, thoughtful reviews of an earlier version of this study by Drake Singleton. The authors acknowledge funding for this work through U.S. Geological Survey award number G15AP00042. Any use of trade, firm, or product names is for descriptive purposes only and does not imply endorsement by the U.S. Government.

REFERENCES CITED

Barcheck, G., Abers, G.A., Adams, A.N., Bécel, A., Collins, J., Gaherty, J.B., Haeussler, P.J., Li, Z., Moore, G., Onyango, E., Roland, E., Sampson, D.E., Schwartz, S.Y., Sheehan, A.F., Shillington, D.J., Shore, P.J., Webb, S., Wiens, D.A., and Worthington, L.L., 2020, The Alaska Amphibious Community Seismic Experiment: Seismological Research Letters, v. 91, no. 6, https://doi.org/10.1785/0220200189.

Bassett, D., and Watts, A.B., 2015, Gravity anomalies, crustal structure, and seismicity at subduction zones: 1. Seafloor roughness and subducting relief: Geochemistry, Geophysics,

Geosystems, v. 16, p. 1508–1540, https://doi.org/10.1002/2014GC005684.
Bécel, A., et al., 2017, Tsunamigenic structures in a creeping section of the Alaska subduction zone: Nature Geoscience, v. 10, no. 8, p. 609–613, https://doi.org/10.1038/ngeo2990.
Blakely, R.J., 1996, Potential Theory in Gravity and Magnetic Applications: Cambridge University Press, 464 p.
Bradley, D., Kusky, T., Haeussler, P., Goldfarb, R., Miller, M., Dumoulin, J., Nelson, S.W., and Karl, S., 2003, Geologic signature of an early Tertiary ridge subduction in Alaska, *in* Sisson, V.B., Roeske, S.M., and Pavlis, T.L., eds., Geology of the Transpressional Oregon Developed during Trench Interaction along the North Pacific Margin: Geological Society of America Special Paper 371, p. 19–49, https://doi.org/10.1130/0-8137-2371-X.19.
Briggs, R.W., Engelhart, S.E., Nelson, A.R., Dura, T., Kemp, A.C., Haeussler, P.J., Corbett, D.R., Angster, S.J., and Bradley, L.-A., 2014, Uplift and subsidence reveal a nonpersistent megathrust rupture boundary (Sitkinak Island, Alaska): Geophysical Research Letters, v. 41, p. 2289–2296, https://doi.org/10.1002/2014GL059380.
Brocher, T.M., Fuis, G.S., Fisher, M.A., Plafker, G., Moses, M.J., Taber, J.J., and Christensen, N.I., 1994, Mapping the megathrust beneath the northern Gulf of Alaska using wide-angle seismic data: Journal of Geophysical Research, v. 99, p. 11,663–11,686, https://doi.org/10.1029/94JB00111.
Bruns, T.R., 1983, Model for the origin of the Yakutat block, an accreting terrane in the northern Gulf of Alaska: Geology, v. 11, no. 12, p. 718–721, https://doi.org/10.1130/0091-7613(1983)11<718:MFTOOT>2.0.CO;2.
Burns, L.E., Pessel, G.H., Little, T.A., Pavlis, T.L., Newberry, R.J., Winkler, G.R., and Decker, J., 1991, Geology of the northern Chugach Mountains, south-central Alaska: State of Alaska Division of Geological and Geophysical Surveys Professional Report 94, 63 p.
Carlson, P.R., and Molnia, B.F., 1975, Preliminary isopach map of Holocene sediments, northern Gulf of Alaska: U.S. Geological Survey Open-File Report 75-507, 1 map sheet, scale 1:500,000.
Carver, G., and Plafker, G., 2008, Paleoseismicity and neotectonics of the Aleutian Subduction Zone—An overview, *in* Freymueller, J.T., et al., eds., Active Tectonics and Seismic Potential of Alaska: Geophysical Monograph 179: Washington, D.C., American Geophysical Union, p. 43–63, https://doi.org/10.1029/179GM03.
Carver, G., Sauber, J., Lettis, W., Witter, R., and Whitney, B., 2008, Active Faults on Northeastern Kodiak Island, Alaska, *in* Freymueller, J.T., et al., eds., Active Tectonics and Seismic Potential of Alaska, Geophysical Monograph 179: Washington, D.C., American Geophysical Union, p. 167–184, https://doi.org/10.1029/179GM09.
Cohen, S.C., and Freymueller, J.T., 2004, Crustal deformation in the south central Alaska subduction zone: Advances in Geophysics, v. 47, p. 1–63, https://doi.org/10.1016/S0065-2687(04)47001-0.
Crameri, F., and Shephard, G.E., 2018, Scientific colour maps (7.0.1): Zenodo, https://doi.org/10.5281/zenodo.1243862 (accessed November 2021).
Doser, D., 2005, Historical Seismicity (1918–1964) of the Kodiak Island Region: Bulletin of the Seismological Society of America, v. 95, no. 3, p. 878–895, https://doi.org/10.1785/0120040175.
Doser, D., Brown, W.A., and Velasquez, M., 2002, Seismicity of the Kodiak Island region (1964–2001) and its relation to the 1964 Great Alaska Earthquake: Bulletin of the Seismological Society of America, v. 92, p. 3269–3292, https://doi.org/10.1785/0120010280.
Eberhart-Phillips, D., Christensen, D.H., Brocher, T.M., Hansen, R., Ruppert, N.A., Haeussler, P.J., and Abers, G.A., 2006, Imaging the transition from Aleutian subduction to Yakutat collision in central Alaska, with local earthquakes and active source data: Journal of Geophysical Research, v. 111, B11303, https://doi.org/10.1029/2005JB004240.
Finn, S.P., Liberty, L.M., Haeussler, P.J., and Pratt, T.L., 2015, Landslides and megathrust splay faults captured by the late Holocene sediment record of eastern Prince William Sound, Alaska: Bulletin of the Seismological Society of America, v. 105, no. 5, p. 2343–2353, https://doi.org/10.1785/0120140273.
Freymueller, J.T., Woodard, H., Cohen, S.C., Cross, R., Elliott, J., Larsen, C.F., Hreinsdóttir, S., and Zweck, C., 2008, Active deformation processes in Alaska, based on 15 years of GPS measurements, *in* Freymueller, J.T., Haeussler, P.J., Wesson, R.L., and Ekström, G., eds., Active Tectonics and Seismic Potential of Alaska: Geophysical Monograph 179: Washington, D.C., American Geophysical Union, p. 1–42, https://doi.org/10.1029/179GM02.
Fisher, M.A., 1980, Petroleum geology of Kodiak shelf, Alaska: American Association of Petroleum Geologists Bulletin, v. 64, no. 8, p. 1140–1157.
Fisher, M.A., and von Huene, R., 1980, Structure of the upper Cenozoic strata beneath Kodiak shelf, Alaska: American Association of Petroleum Geologists Bulletin, v. 64, p. 1014–1033.
Fruehn, J., von Huene, R., and Fisher, M., 1999, Accretion in the wake of terrane collision: The Neogene accretionary wedge off Kenai Peninsula, Alaska: Tectonics, v. 18, p. 263–277, https://doi.org/10.1029/1998TC900021.
Fuller, C.W., Willett, S.D., and Brandon, M.T., 2006, Formation of forearc basins and their influence on subduction zone earthquakes: Geology, v. 34, no. 2, p. 65–68, https://doi.org/10.1130/G21828.1.
Grantz, A., Zietz, I., and Andreasen, G.E., 1963, An aeromagnetic reconnaissance of the Cook Inlet area, Alaska: U.S. Geological Survey Professional Paper 316-G, p. 117–134.
Gulick, S.P.S., Jaeger, J.M., Mix, A.C., Asahi, H., Bahlburg, H., Belanger, C.L., and Swartz, J.M., 2015, Mid-Pleistocene climate transition drives net mass loss from rapidly uplifting St. Elias Mountains, Alaska: Proceedings of the National Academy of Sciences of the United States of America, v. 112, p. 15,042–15,047, https://doi.org/10.1073/pnas.1512549112.
Gutscher, M.A., Kukowski, N., Malavieille, J., and Lallemand, S., 1998, Episodic imbricate thrusting and underthrusting: Analog experiments and mechanical analysis applied to the Alaskan accretionary wedge: Journal of Geophysical Research, v. 103, p. 10,161–10,176, https://doi.org/10.1029/97JB03541.
Haeussler, P.J., Armstrong, P.A., Liberty, L.M., Ferguson, K.M., Finn, S.P., Arkle, J.C., and Pratt, T.L., 2015, Focused exhumation along megathrust splay faults in Prince William Sound, Alaska: Quaternary Science Reviews, v. 113, p. 8–22, https://doi.org/10.1016/j.quascirev.2014.10.013.
Hayes, G.P., Moore, G.L., Portner, D.E., Hearne, M., Flamme, H., Furtney, M., and Smoczyk, G.M., 2018, Slab2—A comprehensive subduction zone geometry model: Science, v. 362, p. 58–61, https://doi.org/10.1126/science.aat4723.
Hutchinson, I., and Crowell, A., 2007, Recurrence and extent of great earthquakes in southern Alaska during the late Holocene from an analysis of the radiocarbon record of land-level change and village abandonment: Radiocarbon, v. 49, no. 3, p. 1323–1385, https://doi.org/10.1017/S0033822200043198.
Ichinose, G., Somerville, P., Thio, H.K., Graves, R., and O'Connell, D., 2007, Rupture process of the 1964 Prince William Sound, Alaska, earthquake from the combined inversion of seismic, tsunami, and geodetic data: Journal of Geophysical Research, v. 112, https://doi.org/10.1029/2006JB004728.
Johnson, J.M., Satake, K., Holdahl, S.R., and Sauber, J., 1996, The 1964 Prince William Sound earthquake: Joint inversion of tsunami and geodetic data: Journal of Geophysical Research, v. 101, p. 523–532, https://doi.org/10.1029/95JB02806.
Kachadoorian, R., and Plafker, G., 1967, Effects of the earthquake of March 27, 1964 on the communities of Kodiak and nearby islands: U.S. Geological Survey Professional Paper 542-F, p. F1–F41, https://doi.org/10.3133/pp542F.
Kaufman, D.S., and Manley, W.F., 2004, Pleistocene maximum and Late Wisconsin glacier extents across Alaska, U.S.A., *in* Ehlers, J., and Gibbard, P.L., eds., Quaternary Glaciations—Extent and Chronology, Part II: North America: Developments in Quaternary Science, v. 2: Amsterdam, Elsevier, p. 9–27, https://doi.org/10.1016/S1571-0866(04)80182-9.
Kaufman, D.S., Young, N.E., Briner, J.P., and Manley, W.F., 2011, Alaska palaeo-glacier atlas (version 2): Developments in Quaternary Sciences, v. 15, p. 427–445, https://doi.org/10.1016/B978-0-444-53447-7.00033-7.
Kelsey, H.M., Witter, R.C., Engelhart, S.E., Briggs, R., Nelson, A., Haeussler, P.J., and Corbett, D.R., 2015, Beach ridges as paleoseismic indicators of abrupt coast subsidence during subduction zone earthquakes, and implications for Alaska-Aleutian subduction zone paleoseismology, southeast coast of the Kenai Peninsula, Alaska: Quaternary Science Reviews, v. 113, p. 147–158, https://doi.org/10.1016/j.quascirev.2015.01.006.
Kim, Y., Abers, G.A., Li, J., Christensen, D., Calkins, J., and Rondenay, S., 2014, Alaska Megathrust 2: Imaging the megathrust zone and Yakutat/Pacific plate interface in the Alaska subduction zone: Journal of Geophysical Research, v. 119, p. 1924–1941, https://doi.org/10.1002/2013JB010581.
Lamb, H., 1932, Hydrodynamics (6th edition): Cambridge, UK, Cambridge University Press, p. 1–8.
Li, J., Shillington, D.J., Saffer, D.M., Bécel, A., Nedimović, M.R., Kuehn, H., Webb, S.C., Keranen, K.M., and Abers, G.A., 2018, Connections between subducted sediment, pore-fluid pressure, and earthquake behavior along the Alaska megathrust: Geology, v. 46, no. 4, p. 299–302, https://doi.org/10.1130/G39557.1.
Li, S., Freymueller, J., and McCaffrey, R., 2016, Slow slip events and time-dependent variations in locking beneath Lower Cook Inlet of the Alaska-Aleutian subduction zone: Journal of Geophysical Research. Solid Earth, v. 121, no. 2, p. 1060–1079, https://doi.org/10.1002/2015JB012491.
Liberty, L.M., 2013, Retrieval, Processing, Interpretation and Cataloging of Legacy Seismic Reflection Data, Gulf of Alaska: U.S. Geological Survey Final Technical Report G12AP20078, 17 p., https://earthquake.usgs.gov/cfusion/external_grants/reports/G12AP20078.pdf.
Liberty, L.M., 2015, Near Surface Expression of Megathrust Splay Faults, Western Gulf of Alaska: U.S. Geological Survey Final

Technical Report #G13AP00021, 17 p., https://earthquake.usgs.gov/cfusion/external_grants/reports/G13AP00021.pdf.
Liberty, L.M., and Ramos, M.D., 2016, Co-seismic rupture patterns over multiple earthquake cycles near Kodiak Island: A collaborative project with USGS personnel: U.S. Geological Survey Final Technical Report #G13AP00021, 17 p., https://earthquake.usgs.gov/cfusion/external_grants/reports/G15AP00042.pdf.
Liberty, L.M., Finn, S.P., Haeussler, P.J., Pratt, T.L., and Peterson, A., 2013, Megathrust splay faults at the focus of the Prince William Sound asperity, Alaska: Journal of Geophysical Research, v. 118, no. 10, p. 5428–5441, https://doi.org/10.1002/jgrb.50372.
Liberty, L.M., Brothers, D.S., and Haeussler, P.J., 2019, Tsunamigenic splay faults imply a long-term asperity in southern Prince William Sound, Alaska: Geophysical Research Letters, v. 46, p. 3764–3772, https://doi.org/10.1029/2018GL081528.
Mankhemthong, N., Doser, D.I., and Pavlis, T.L., 2013, Interpretation of gravity and magnetic data and development of two-dimensional cross-sectional models for the border ranges fault system, south-central Alaska: Geosphere, v. 9, no. 2, p. 242–259, https://doi.org/10.1130/GES00833.1.
Maus, S., 2009, EMAG2: Earth Magnetic Anomaly Grid (2-arc-minute resolution): Version 2: NOAA National Centers for Environmental Information, https://doi.org/10.7289/V5MW2F2P (accessed May 2016).
Menard, H.W., and Atwater, T., 1969, Origin of fracture zone topography: Nature, v. 222, no. 5198, p. 1037–1040, https://doi.org/10.1038/2221037a0.
Meyer, B., Saltus, R., and Chulliat, A., 2017, EMAG2v3: Earth Magnetic Anomaly Grid (2-arc-minute resolution). Version 3: NOAA National Centers for Environmental Information (accessed 2 July 2021).
Moore, J.C., Bryne, T., Plumely, P.W., Reid, M., Gibbons, H., and Coe, R.S., 1983, Paleogene evolution of the Kodiak Islands, Alaska: Consequences of ridge-trench interaction in a more southerly latitude: Tectonics, v. 2, p. 265–293, https://doi.org/10.1029/TC002i003p00265.
Moore, J.C., Diebold, J., Fisher, M.A., Sample, J., Brocher, T., Talwani, M., Ewing, J., von Huene, R., Rose, C., Stone, D., Stevens, C., and Sawyer, D., 1991, EDGE deep seismic reflection transect of the eastern Aleutian arc-trench layered lower crust reveals underplating and continental growth: Geology, v. 19, no. 5, p. 420–424, https://doi.org/10.1130/0091-7613(1991)019<0420:EDSRTO>2.3.CO;2.
Naugler, F.P., and Wageman, J.M., 1973, Gulf of Alaska: Magnetic anomalies, fracture zones, and plate interaction: Geological Society of America Bulletin, v. 84, p. 1575–1584, https://doi.org/10.1130/0016-7606(1973)84<1575:GOAMAF>2.0.CO;2.
Nishenko, S.P., and Jacob, K.H., 1990, Seismic potential of the Queen Charlotte-Alaska-Aleutian seismic zone: Journal of Geophysical Research, v. 95, p. 2511–2532, https://doi.org/10.1029/JB095iB03p02511.
NOAA National Centers for Environmental Information, 2004, Multibeam Bathymetry Database (MBBDB): NOAA National Centers for Environmental Information (accessed February 2017).
NOAA National Geophysical Data Center, 2009, Southern Alaska Coastal Relief Model: NOAA National Centers for Environmental Information, https://doi.org/10.7289/V58G8HMQ (last accessed January 2016).
Pavlis, T.L., and Roeske, S.M., 2007, The Border Ranges fault system, southern Alaska, *in* Ridgway, K.D., et al., eds., Tectonic Growth of a Collisional Continental Margin: Crustal Evolution of Southern Alaska: Geological Society of America Special Paper 431, p. 95–128, https://doi.org/10.1130/2007.2431(05).
Peltier, W.R., and Fairbanks, R.G, 2006, Global glacial ice volume and Last Glacial Maximum duration from an extended Barbados sea level record: Quaternary Science Reviews, v. 25, p. 3322–3337, https://doi.org/10.1016/j.quascirev.2006.04.010.
Plafker, G., 1969, Tectonics of the March 27, 1964 Alaska earthquake: U.S. Geological Survey Professional Paper 543-I, 74 p.
Plafker, G., and Berg, H.C., eds., 1994, The Geology of Alaska: Decade of North American Geology: Boulder, Colorado, Geological Society of America, v. G-1, 1068 p.
Porto, N.M., and Fitzenz, D.D., 2016, An alternative segmentation model for the Alaskan Aleutian megathrust: Bulletin of the Seismological Society of America, v. 106, no. 3, p. 1125–1132, https://doi.org/10.1785/0120150235.
Reece, R.S., Gulick, S.P.S., Horton, B.K., Christeson, G.L., and Worthington, L.L., 2011, Tectonic and climatic influence on the evolution of the Surveyor fan and channel system, Gulf of Alaska: Geosphere, v. 7, no. 4, p. 830–844, https://doi.org/10.1130/GES00654.1.
Robinson, D.P., and Watts, A.B., 2006, Earthquake rupture stalled by a subducting fracture zone: Science, v. 312, p. 1203–1205, https://doi.org/10.1126/science.1125771.
Ryan, H.F., von Huene, R., Wells, R.E., Scholl, D.W., Kirby, S., and Draut, A.E., 2011, History of earthquakes and tsunamis along the eastern Aleutian-Alaska megathrust, with implications for tsunami hazards in the California continental borderland: U.S. Geological Survey Professional Paper 1795-A, 31 p.
Saltus, R.W., Hudson, T.L., and Wilson, F.H., 2007, The geophysical character of southern Alaska—Implications for crustal evolution, *in* Ridgway, K.D., Trop, J.M., Glen, J.M.G., and O'Neill, J.M., eds., Tectonic Growth of a Collisional Continental Margin: Crustal Evolution of Southern Alaska, USA: Geological Society of America Special Paper 431, p. 1–20, https://doi.org/10.1130/2007.2431(01).
Sandwell, D.T., 1984, Thermomechanical evolution of oceanic fracture zones: Journal of Geophysical Research, v. 89, p. 11,401–11,413, https://doi.org/10.1029/JB089iB13p11401.
Sandwell, D.T., Müller, R.D., Smith, W.H.F., Garcia, E., and Francis, R., 2014, New global marine gravity model from CryoSat-2 and Jason-1 reveals buried tectonic structure: Science, v. 346, no. 6205, p. 65–67, https://doi.org/10.1126/science.1258213.
Sauber, J., Carver, G., Cohen, S., and King, R., 2006, Crustal deformation and the seismic cycle across the Kodiak Islands, Alaska: Journal of Geophysical Research, v. 111, B02403, https://doi.org/10.1029/2005JB003626.
Shennan, I., Barlow, N., Carver, G., Davies, F., Garrett, E., and Hocking, E., 2014, Great tsunamigenic earthquakes during the past 1000 yr on the Alaska megathrust: Geology, v. 42, no. 8, p. 687–690, https://doi.org/10.1130/G35797.1.
Shennan, I., Brader, M.D., Barlow, N.L.M., Davies, F.P., Longley, C., and Tunstall, N., 2018, Late Holocene paleoseismology of Shuyak Island, Alaska: Quaternary Science Reviews, v. 201, p. 380–395, https://doi.org/10.1016/j.quascirev.2018.10.028.
Shillington, D.J., Bécel, A., Nedimović, M.R., Kuehn, H., Webb, S.C., Abers, G.A., Keranen, K.M., Li, J., Delecluse, M., and Mattei-Salicrup, G.A., 2015, Link between plate fabric, hydration and subduction zone seismicity in Alaska: Nature Geoscience, v. 8, p. 961–964, https://doi.org/10.1038/ngeo2586.
Smith, W.H.F., and Sandwell, D.T., 1997, Global seafloor topography from satellite altimetry and ship depth soundings: Science, v. 277, p. 1956–1962, https://doi.org/10.1126/science.277.5334.1956.
Song, T.A., and Simons, M., 2003, Large trench-parallel gravity variations predict seismogenic behavior in subduction zones: Science, v. 301, p. 630–633, https://doi.org/10.1126/science.1085557.
Suito, H., and Freymueller, J.T., 2009, A viscoelastic and afterslip postseismic deformation model for the 1964 Alaska earthquake: Journal of Geophysical Research, v. 114, https://doi.org/10.1029/2008JB005954.
Suleimani, E., and Freymueller, J.T., 2020, Near-field modeling of the 1964 Alaska tsunami: The role of splay faults and horizontal displacements: Journal of Geophysical Research. Solid Earth, v. 125, p. 1–23, https://doi.org/10.1029/2020JB019620.
von Huene, R., Hampton, M., Fisher, M., Varchol, D., and Cochrane, G., 1980, Map showing near-surface geologic structures of Kodiak Shelf, Alaska: U.S. Geological Survey Miscellaneous Field Studies Map MF-1200, 1 sheet, 1:500,000 scale.
von Huene, R., Fisher, M.A., and Bruns, T.R., 1987, Geology and evolution of the Kodiak margin, Gulf of Alaska, *in* Scholl, D.W., Grantz, A., and Vedder, J.G., eds., Geology and Resource Potential of the Continental Margin of Western North America and Adjacent Ocean Basins—Beaufort Sea to Baja California: Houston, Texas, Circum-Pacific Council for Energy and Mineral Resources, p. 191–212.
von Huene, R., Klaeschen, D., and Fruehn, J., 1999, Relation between the subducting plate and seismicity associated with the great 1964 Alaska Earthquake: Pure and Applied Geophysics, v. 154, p. 575–591, https://doi.org/10.1007/s000240050245.
von Huene, R., Miller, J.J., and Weinrebe, W., 2012, Subducting plate geology in three great earthquake ruptures of the western Alaska margin, Kodiak to Unimak: Geosphere, v. 8, no. 3, p. 628–644, https://doi.org/10.1130/GES00715.1.
Wang, K., and Hu, Y., 2006, Accretionary prisms in subduction earthquake cycles: The theory of dynamic Coulomb wedge: Journal of Geophysical Research, v. 111, B06410, https://doi.org/10.1029/2005JB004094.
Wells, D.L., and Coppersmith, K.J., 1994, New empirical relationships among magnitude, rupture length, rupture width, rupture area, and surface displacement: Bulletin of the Seismological Society of America, v. 84, no. 4, p. 974–1002.
Wells, R.E., Blakely, R.J., Sugiyama, Y., Scholl, D.W., and Dinterman, P.A., 2003, Correction to "Basin-centered asperities in great subduction zone earthquakes: A link between slip, subsidence, and subduction erosion?": Journal of Geophysical Research, v. 108, https://doi.org/10.1029/2003JB002880.
Ye, S., Flueh, E.R., Klaeschen, D., and von Huene, R., 1997, Crustal structure along the EDGE transect beneath the Kodiak shelf off Alaska derived from OBH seismic refraction data: Geophysical Journal International, v. 130, p. 283–302, https://doi.org/10.1111/j.1365-246X.1997.tb05648.x.
Zimmermann, M., Prescott, M.M., and Haeussler, P.J., 2019, Bathymetry and geomorphology of Shelikof Strait and the Western Gulf of Alaska: Geosciences, v. 9, no. 10, p. 409, https://doi.org/10.3390/geosciences9100409.
Zweck, C., Freymueller, J.T., and Cohen, S.C., 2002, Three-dimensional elastic dislocation modeling of the postseismic response to the 1964 Alaska earthquake: Journal of Geophysical Research, v. 107, p. ECV 1-1–ECV 1-11, https://doi.org/10.1029/2001JB000409.